AN ABSTRACT OF THE THESIS OF

Ju Zhou Tao for the degree of Doctor of Philosophy in Chemistry presented on July 10, 2002.

Title: Theory of Negative Thermal Expansion

Abstract approved: Redacted for Privacy
Arthur W. Sleight

Two framework oxide materials of the MO_3 network type have been synthesized and structurally characterized by synchrotron and X-ray powder diffraction and the Rietveld method in the temperature range 25~500 K. The results show one of them to be a low thermal expansion material.

Theoretical studies of negative thermal expansion (NTE) in framework oxides were conducted with two methods, geometrical modeling by Rigid Unit Mode (RUM) method and lattice dynamic calculations by free energy minimization (FEM) method, the results are compared with each other as well as with experimental observations.

RUM analysis of all five types of framework oxide structures negates any simple and direct correlation between presence or absence of RUMs in a structure and the sign of its thermal expansion. Instead, results suggest that NTE of a crystalline solid can not be explained by pure geometrical considerations over its

structure alone, and for a better understanding of structure-relationship in negative thermal expansion structures, specific interatomic interactions present in each one must be brought in explicitly.

FEM calculation of two negative thermal expansion structures indicates on a structure by structure basis NTE could be predicted and understood within the Grüneisen model, which attributes NTE of a structure to special vibration modes in a structure that softens when the lattice shrinks. The soft NTE modes are, however, not necessarily RUM or RUM like vibration motions.

Theory of Negative Thermal Expansion

by

Ju Zhou Tao

A THESIS

Submitted to

Oregon State University

In partial fulfillment of
The requirement for the degree of

Doctor of Philosophy

Presented July 10, 2002
Commencement June 2003

Doctor of Philosophy thesis of Ju Zhou Tao presented on July 10, 2002.

APPROVED:

Redacted for Privacy

Major Professor, representing Chemistry

Redacted for Privacy

Chair of the Department of Chemistry

Redacted for Privacy

Dean of Graduate School

I understand that my thesis will become part of the permanent collection of Oregon State University libraries. My signature below authorizes release of my thesis to any reader upon request.

Redacted for Privacy

Ju Zhou Tao, Author

ACKNOWLEDGEMENT

My study and work at Oregon State University has been a wonderful period of concentrated professional development, free intellectual exploration and multifarious social experiences. In hinder sight I didn't do as much as what I had hoped (could one ever do?), but for sure I did far more than what I had expected and had a great time!

To that I am indebted to many. First and foremost is my advisor, Dr. Arthur W. Sleight, whose extraordinary scientific intuition, vivid technology flair and high research standards I much admire and hope to emulate in my future career; whose personal kindness and generosity (and hospitality of his scenery homes!) I much enjoyed, and for which I will be always grateful. It is my fortune to be able to have him, a leading (solid state) chemist in the world and real scientist in heart, as my graduate mentor. I hope he found some contents of this thesis interesting, as well as never got tired of answering all my questions in the future.

Sleight group's labs in the northeast wing of second floor of Gilbert Hall have been my second home for the past six years also, which I shared with many past and present members of the group: Nazy, Matt, Maddy, Ivana, Pat, John, Mary, Seung-Tae, Martin, Corrine, Claire, Xinghua, Svetlana, Dunkung, Tammy, Jun, Xiumei, Niangao, Kamiswari, Raje, Vanaje, Paul, Qingnan. Some of them showed me great kindness, others offered help when it was most needed, and from each one of them I learned something new.

Dr. Martin Attfield helped me collect temperature varying synchrotron diffraction data on TaO_2F and NbO_2F during our research trip to the NSLS national lab on the Long Island, New York, which as an eye-opening experience for me would always be cherished; Dr. Alex Yokochi kindly helped me collect temperature varying X-ray data on our Inel PSD diffractometer; Dr. Martin Dove of University of Cambridge, UK generously provided me source codes of CRUSH program used for RUM modeling, Dr. Julian Gale of Imperial College of Science, Technology and Medicine of UK kindly offered me source codes of GULP program used for lattice dynamic calculations, and even revised it for my special need. This thesis would be unrecognizable as the current form without their assistance, which is deeply appreciated.

I am also indebted to many a friend within the OSU community, Marcus, Jeff, Engelene, Sherry, Dong, Greg, (Big) Eric, Ainong, Qin, Yuan. Many a teacher taught me classes in different departments, including all departmental members of my graduate committee: Dr. Nibler, Dr. Keszler and Dr. Kong. The wonderful time I was privileged to share with all of them around the campus would always be relived in memory.

Without my family, Father, Mother, and my younger sister behind me in China, life and work at US for me is not possible. In certain sociological sense and true Chinese tradition, they are unwritten coauthors of this text. To their love I would forever be indebted.

TABLE OF CONTENTS

TABLE OF CONTENTS (Continued)

TABLE OF CONTENTS (Continued)

Page

LIST OF FIGURES

LIST OF FIGURES (Continued)

LIST OF TABLES

Theory of Negative Thermal Expansion

Chapter 1

Introduction to Thermal Expansion

1.1. Negative Thermal Expansion

The term "thermal expansion" reflects both the common sense knowledge throughout human material history that matter (air, metals, common ceramics and building materials) expands when it is hot or heated; and more recent scientific observations that volumes of materials (gases, liquids, solids) increase at elevated temperature. Indeed, the dictum "expanding when heated and shrinking when cooled" was once written into school texts as a simple and straightforward empirical law of nature.

But this was found to be pseudo-knowledge. First, fundamental laws of thermodynamics and statistical mechanics don't dictate signs of thermal expansion, unlike other more fundamental thermodynamic quantities: entropy of a system is always positive given its statistical origin; thermal capacity and compressibility of a structure has to be positive too (otherwise it would become unstable and self-explosive); and total energy of a condensed phase is always negative (compared to the state of an assembly of isolated atomic or subatomic particles, which is usually

the energy reference level in any practical calculations). The difference highlights the nature of thermal expansion being not so much a basic physical quantity as that of a material property.

Secondly, through indirect deductions or direct measurements of thermal expansions of many a crystalline material a few have been discovered to experience negative thermal expansion (NTE), i.e., they contract at higher temperatures. Certain perovskite ferroelectrics (1), tetrahedral semiconductors such as Si, Ge, GaAs, ZnSe, GaP, and Cu_2O (2), ice (3), amorphous SiO_2 show this behavior at low temperatures, ZrV_2O_7 (4), quartz (5), cristobalite (6) and faujasite at high temperature.

Finally, systematical work conducted with latest scientific methods in solid state science discovered many more crystalline materials with negative thermal expansion property along the whole temperature range from close to 0 K up to well above 1000 K (highest around 1500 K so far). Compared to most crystalline materials with "normal" positive thermal expansion they are still exceptions, but NTE certainly shouldn't be viewed as an anomaly any more, and within certain structure types such as framework silicates and aluminophosphates there are signs it may even be widely occurring (7, 8).

1.2. Researches on NTE

Thermal expansion behavior of materials is important or even crucial in many industrial processes and practical applications, such as matching thermal expansion of circuit boards and heat sinks to Si, dental restorations, zero thermal expansion for telescope mirrors, laser devices, optical gadgets, athermalization of fiber optic Bragg gratings etc. The prospect of combining NTE materials with other polymer, metal or ceramic materials to manufacture composites with designed thermal expansion coefficients, no matter it being negative, positive or almost zero, is fascinating and exciting.

Researches on NTE materials and properties are generally conducted along one of two lines: one with the emphasis on material-structure relationships centered on the search for new structures that show negative thermal expansion, and preparation of materials with these desired structures; the other focuses on structure-(thermal expansion) property relationship in attempts to understand NTE better, with the hope of bringing the understanding back into first line of work, ideally in the form of simple empirical rules or models, to help discover and synthesize more NTE materials. Clearly two lines of work are not independent and thoroughly intertwined, with the former trying to meet the challenge: "what (other) structures/materials show NTE?", and the latter attempting to answer the question: "why these structures/materials show NTE but not others?"

Between ZrV_2O_7 and SiO_2 faujasite, two materials among the first found to experience negative thermal expansion, one striking feature is shared that in both structures oxygen atoms are two coordinated bridging two cations to form linear or close to linear M-O-M bonds, or in terms of network connectivity, all metal-oxygen polyhedra share corners only. Transverse vibration motions of oxygen atoms to the bond direction are expected to be low energy and to decrease interatomic distances between two bonded cations by simple geometrical arguments as illustrated in Figure 1.1:

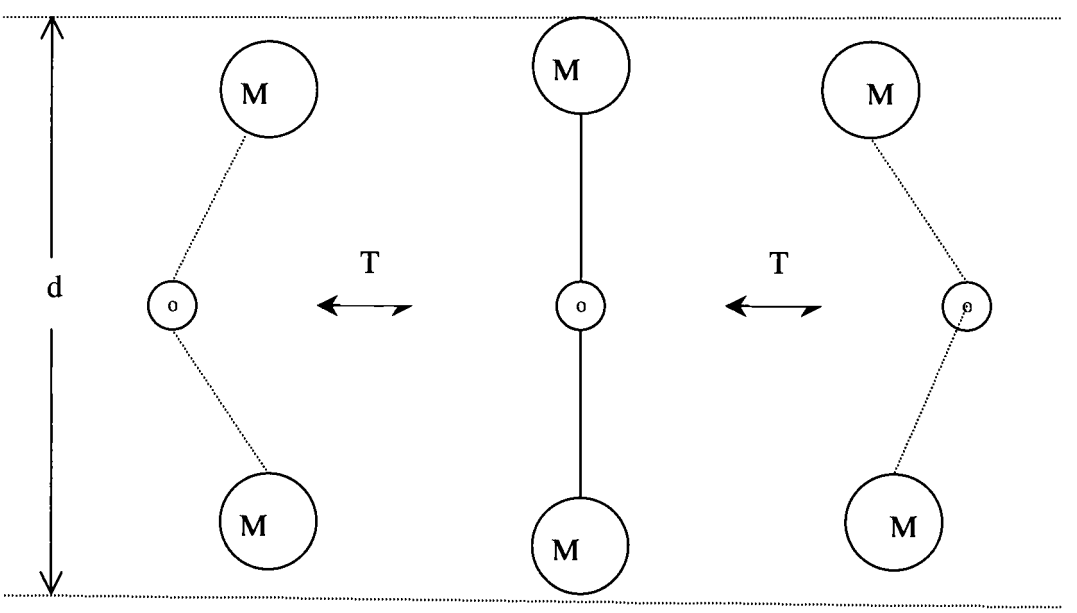

Figure 1.1. Decreased interatomic distances due to thermal vibration of 2-coordinated Oxygen atoms.

At higher temperatures these low energy vibration modes are expected to be excited more so than at lower temperature, leading to decreased cation distances in a structure on average, i.e., negative thermal expansion of the material.

This working hypothesis appears to be first advanced to explain occurrence of negative thermal expansion in ZrV_2O_7 (4), and becomes the starting point for further ongoing research efforts on NTE oxide materials, of which this thesis work is a part.

1.3. Material-Structure Line of Work on NTE

Two most common structure building blocks in framework oxides are tetrahedra (AO_2 network such as SiO_2) and octahedra (MO_3 network such as WO_3). If we require all oxygen atoms in a structure are corner sharing ones connecting two polyhedra, then the generic composition of a framework structure is $A_xM_yO_{2x+3y}$. With further constraints of possible combinations of cation and anion valencies (Oxygen is always –2, A and M as cations are no more than +6), the formula generates five types of networks that are known to exist: AO_2, A_2MO_7, $A_3M_2O_{12}$, AMO_5, MO_3. These are five types of framework structures within which searches for more NTE materials have been carried out:

1.3.1. Five Types of Networks

ZrP_2O_7, ZrV_2O_7, HfV_2O_7 and HfP_2O_7 are four materials with the A_2MO_7 network structure, with A being +5 P or V and M being +4 Zr or Hf. In this structure each MO_3 octahedra shares corners with six AO_2 tetrahedra and each AO_2 tetrahedron shares corners with three MO_3 octahedral and one other AO_2 tetrahedron. These materials typically undergo phase transitions and show NTE in higher temperature higher symmetry cubic phases (4).

If AO_2 tetrahedra in this network only share corners with three MO_3 octahedra and leave one corner linkage free, the resulted structure is that of cubic alpha-ZrW_2O_8, which is shown to experience large isotropic thermal expansion over a wide temperature range from close to 0 K up to about 1500 K (9) Materials with similar structure like $Zr(W/Mo)_2O_8$ have also been synthesized and shown to experience NTE (10, 11).

Within the $A_3M_2O_{12}$ family NTE was found for $Sc_2W_3O_{12}$ (12), $Y_2W_3O_{12}$ and $Lu_2W_3O_{12}$ (13, 14) over specific temperature ranges. The structure consists of a 3-D network of corner-sharing interconnecting WO_2 tetrahedra and MO_3 octahedra, with no linkage between tetrahedral and octahedral themselves. All polyhedra are slightly distorted, however, and symmetry of the structure is orthorhombic at higher temperature and monoclinic at lower temperature across a phase transition.

The huge family of framework silicates and aluminophosphates are well known and well studied AO_2 networks, which consist of almost rigid and ideal SiO_2

tetrahedra (or alternating AlO_2 and PO_2 tetrahedra) interconnecting to each other by sharing corners. Many structures within this type of network are shown or predicted to be NTE: faujasite, $AlPO_4$-17 (15).

For AMO_5 networks a large group of solid compounds also exist, where A could be Nb, Ta, Mo, V, Sb, and M could be P, V, As, Mo. In these structures each MO_3 octahedron share corners with four AO_2 tetrahedra and 2 other octahedra, and each AO_2 tetrahedron with four MO_3 octahedra, overall symmetries varying with structures between tetragonal and monoclinic. The high temperature phase of $NbOPO_4$, $TaOP_4$, and orthorhombic $TaOVO_4$ are found to show negative thermal expansion (16).

The MO_3 network consists of interconnecting corner-sharing metal-oxygen octahedra, which could be ideal as in ReO_3, or distorted as in UO_3 and WO_3. NbO_2F and TaO_2F are two compounds of this network type with ideal polyhedra, their preparation and thermal expansion studies are presented in detail in the next chapter. These two structures show very small thermal expansion of a magnitude comparable to experimental and data analysis errors, therefore we can't say with certainty that they are NTE or not. No other structures of this network are known to experience NTE either.

1.3.2. Preparation of NTE Materials

Since thermal expansion is a thermodynamic property of phases, in general no special requirements are needed for synthesis of NTE materials, as long as crystalline samples could be prepared for structure characterization studies and thermal expansion measurements. Indeed almost all solid state synthesis methods were explored in preparing compounds with structures discussed above: conventional solid state routes for most of them, hydrothermal for $AlPO_4$-17, solution reactions for some $AOMO_4$ structures and $(Nb/Ta)O_2F$, and combustion synthesis as one route for ZrW_2O_8.

1.3.3. Structure Characterization of NTE Materials: Diffraction Techniques

Powder X-ray or neutron diffraction measurements followed by structure refinements using the Rietveld method (17) or whole pattern fitting with the Le Bail method (18) have been well established as a technique to characterize structures of crystalline materials. To study thermal expansion properties of crystalline oxides one only needs to bring in temperature as an experimental variable to measure changes of lattice parameters as a function of temperature.

This method is straightforward and turns out most productive, as illustrated by the sudden "explosion" of the number of NTE structures after 1995. Still it is not

without its own problems: first, commercial powder diffractometers capable of quantitative (means quality of data would be good enough for Rietveld analysis) measurements over a wide temperature range are difficult to come by or maintain, and special research diffractometers utilizing synchrotron or neutron sources with reliable temperature varying function have limited accessibility.

Second and more importantly, studying changes of lattice parameters as a function of temperature requires precise and reliable measurements of lattice parameters of a structure, which can be problematic in certain cases. Powder diffraction measurements only produce structure information through structure refinement or whole pattern fitting of collected diffraction diagram data, but both instrumentation and data analysis processes introduce errors into final experimental values of lattice parameters. If thermal expansion is too small between measurements (and corresponding data analysis) at two different temperatures, either due to very small thermal expansion coefficient or because of small lattice parameters themselves, uncertainties produced by these errors could distort or overwhelm the trend of lattice parameter changes due to thermal expansion, making it difficult to determine if a structure displays NTE.

1.3.4. Direct Measurement of Thermal Expansion: Dilatometry

For materials that could be sintered to form hard and well shaped ceramic bars, direct measurement of thermal expansion could be conducted on a dilatometer which measures length change of the bar during heating and cooling, and coverts it to thermal expansion after proper thermal-analytical corrections. Typical sample size is 5×5×25 mm, and highest working temperature is around 1200 °C. However if a material's thermal expansion is anisotropic enough, i.e., linear thermal expansion coefficients along each one of three crystal lattice directions being vastly different, crystallites in a ceramic body can expand in some directions but contracting in other directions, and microcracks will form on cooling from higher temperature at which the ceramic was consolidated (19). These cracks enlarge on cooling and tend to disappear again on heating, leading to negative thermal expansion of an extrinsic type. This complication is most problemetic for low symmetry materials with highly anisotropic thermal expansion property.

1.4. Structure-Property Relationship in NTE Materials

Fundamental rules of thermodynamics not only do not forbid negative thermal expansion, but also provide the simplest (and easy!) answer to the question why negative thermal expansion occurs: they contract themselves as an adjustment to

higher temperature to keep its (Gibbs) free energy at a minimal! But to understand why only certain materials experience NTE while other materials of similar structure don't, we have to answer the slightly different but much more difficult question how negative thermal expansion occurs, namely what structure features or thermodynamic mechanisms are responsible for it.

1.4.1. Geometrical Considerations

The first proposed mechanism attributed negative thermal expansion in oxides to transverse vibrations of 2-coordinated bridging oxygen atoms in these structures, a lattice vibration mode expected to be low enough in energy to be readily excited leading to decreased lattice parameters on average. This geometrical argument is illustrated in Figure 1.2:

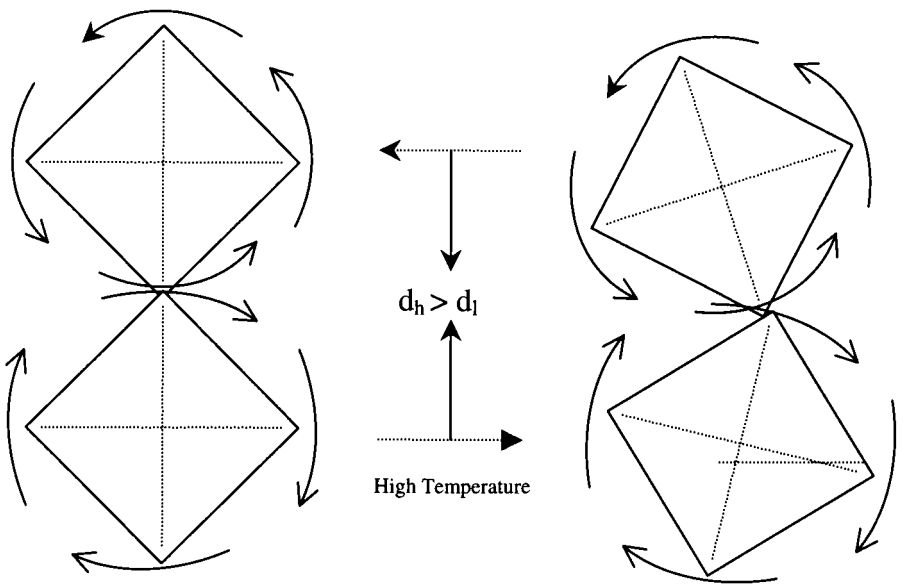

Figure 1.2. A schematic representation of how polyhedral rocking due to thermal vibrations can lead to decreased lattice parameters.

However, several difficulties exist for this physical picture. First is that it could not explain why materials with similar structures of interconnecting corner-sharing metal-oxygen polyhedra networks do not show negative thermal expansion, such as quartz itself before α-β phase transition. To argue that this kind of transverse oxygen modes in some structures might be too high in energy to contribute to NTE weakens its predicting power; second, there is a hidden paradox in this geometrical argument: the physical picture as illustrated in Figure 1.2 presumes the existence of

various vibration modes in a crystal structure with well defined (and fixed) lattice parameters, yet deduction is made from this physical model that lattice parameters will change because of certain special vibration modes among all of them. The last and most serious problem is that some experimental evidence appears to indicate M-O-M linkage can be quite stiff and does not support large transverse motion by oxygen atoms bridging two cations, such as Zr-O-W in ZrW_2O_8, and vibration motions that give rise to NTE do not involve identifiable large transverse vibrations of oxygen atoms in this structure (20).

The transverse oxygen vibration mechanism therefore is more of a working hypothesis, a solid state chemist's tool/trick of trade, that helps to draw attention to one conspicuous structure feature common to many a NTE material: 2-coordinated bridging oxygen atoms. Its value lies more so in the fact that it could help us search for and hit on new NTE structures, as witnessed by many examples of them after 1995, than a strictly physically correct explanation of NTE. Whether there exist NTE oxide materials without linearly (or close to it) bonded oxygen is still an open and interesting question, and what kind of role this structural feature plays in the thermal expansion of known NTE materials is a related and intriguing one too.

One approach in attempts to answer the last question is to quantify the simple geometrical model as illustrated in Figure 1.2, and then apply it to structures with different thermal expansion property. Two methods are currently available: first is Distance Least Square Refinements (DLS), which assigns lattice parameters and symmetry operations to a structure, and adjusts internal atomic coordinates in a unit

cell to match a set of prescribed interatomic distances. This method has been successfully used to model the flexibility of network structures (21), but appears to pose certain difficulties in direct application to study thermal expansion property of a structure. The main reason is probably the method was built to model static geometrical structure, while thermal expansion really has its origin in dynamic atomic motions determined by interatomic interactions in a structure.

The second method is Rigid Unit Mode (RUM) analysis (22), which has its origin in modeling structure-relationship of framework silicates and aluminophosphates. Extending the method to study all types of framework oxides with 2-coordinated oxygen with respect to their thermal expansion properties is a part of this thesis work and would be discussed in detail in Chapter 4.

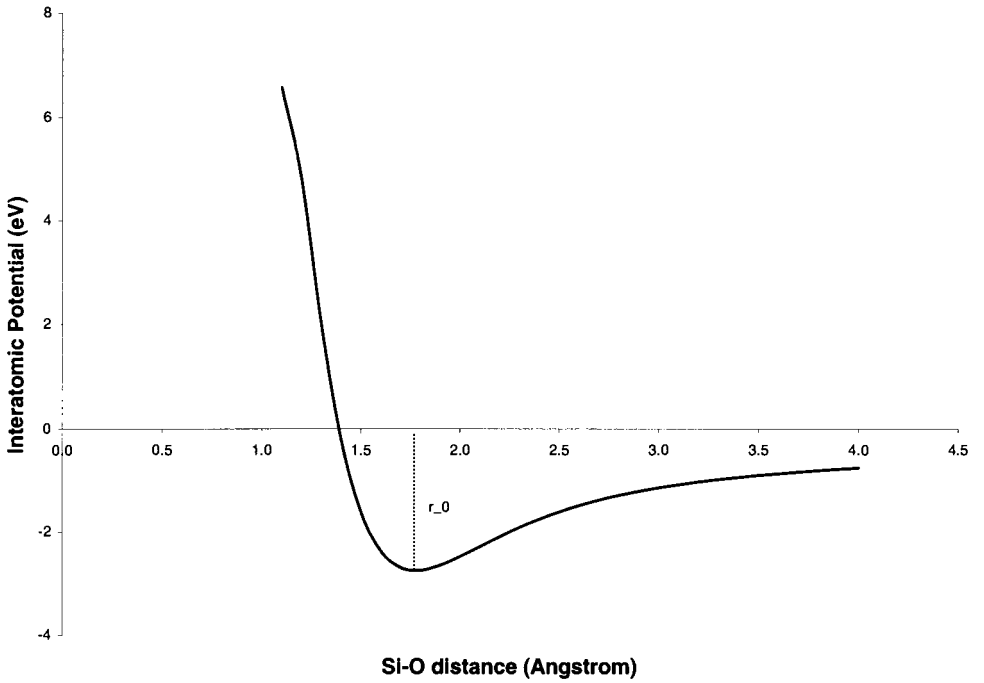

Figure 1.3. Typical 2-body interatomic potential in a crystal structure.

1.4.2. Physical Models

Traditionally thermal expansion was often rationalized by a two-body interatomic potential model as illustrated in Figure 1.3, where at the equilibrium interatomic distance r_0 interatomic potential energy reaches a minimal, and higher energy vibrational states correspond to larger interatomic distances. When temperature is increased the system would spend more time in higher energy states

leading to an increased average interatomic distance, henceforth (positive) thermal expansion.

The appearance of many examples of NTE materials demonstrated insufficiency of this two-body interatomic potential model, which appears to predict positive thermal expansion for any solid and is more suitable to molecular structures with limited number of atoms rather than highly ionic solids with their structures based on an ideal crystal lattice, where equilibrium distances between near neighbor atoms or even neighbor (bonded) atoms are not necessarily the ones decided by two-body interatomic potentials, due to complex many-body interactions existing in a structure. In chapter 4 a two-body interatomic potential model is further utilized to calculate negative thermal expansion of an aluminophosphate $AlPO_4$-17 directly, but the same potential model and method could also be used to simulate positive thermal expansion of other aluminophosphates! This clearly shows NTE can not be rationalized only in terms of two-body interatomic potentials.

For a better theoretical framework within which NTE could be more satisfactorily understood we have to turn to lattice dynamics, where thermal expansion is described by the Grüneisen model (23, 24).

The volumetric thermal expansion is defined as:

$$\alpha = \frac{1}{V}\left(\frac{\partial V}{\partial T}\right)_p \tag{1.1}$$

The partition function for each vibration mode on a crystal lattice can be calculated:

$$z = \sum_{n=0}^{\infty} e^{-\frac{(n+\frac{1}{2})\hbar\omega}{kT}} = \frac{e^{-\frac{1}{2}\frac{\hbar\omega}{kT}}}{1-e^{-\frac{\hbar\omega}{kT}}} \tag{1.2}$$

And its contribution to total Helmhotz free energy is:

$$f = -kT \ln z = \frac{1}{2}\hbar\omega + kT\sum_i \ln(1-e^{\frac{-\hbar\omega}{kT}}) \tag{1.3}$$

Free energy of the lattice is the sum from all vibration modes plus the potential energy from interatomic interactions:

$$F = U + \frac{1}{2}\sum_i \hbar\omega_i + kT\sum_i \ln(1-e^{-\frac{\hbar\omega_i}{kT}}) \tag{1.4}$$

Thermal expansion coefficient from equation (1) can be transformed to:

$$\alpha = \frac{1}{V}\left(\frac{\partial V}{\partial T}\right)_p = -\frac{1}{V}\left(\frac{\partial P}{\partial T}\right)_V\left(\frac{\partial V}{\partial P}\right)_T = K_T\left(\frac{\partial P}{\partial T}\right)_V \tag{1.5}$$

$\left(\frac{\partial P}{\partial T}\right)_V$ term can be calculated from free energy with equation (1.4):

$$P = -\left(\frac{\partial F}{\partial V}\right)_T = -\left(\frac{\partial U}{\partial V}\right)_T - \frac{1}{2}\sum_{q,s}\hbar\left(\frac{\partial \omega(q,s)}{\partial V}\right)_T - \sum_{q,s} n(\omega,T)\hbar\left(\frac{\partial \omega(q,s)}{\partial V}\right) \tag{1.6}$$

With quasi-harmonic approximation U and $\omega(q,s)$ are independent of temperature at constant volume:

$$\left(\frac{\partial P}{\partial T}\right)_V = -\hbar\sum_{q,s}\frac{\partial n(\omega,T)}{\partial T}\frac{\partial \omega(q,s)}{\partial V} \tag{1.7}$$

where q is the wave-vector, s the degrees of vibration freedom in a primitive unit cell, n occupancy for the vibration state by Bose-Einstein statistics. Introducing notation $C_{q,s}$ which is contribution of one vibration mode to the heat capacity:

$$C_{q,s} = \hbar\omega(T)\frac{\partial n(\omega,T)}{\partial T} \tag{1.8}$$

Thermal expansion coefficient becomes:

$$\alpha = -k_T\sum_{q,s}\frac{C_{q,s}}{\omega(q,s)}\frac{\partial \omega(q,s)}{\partial V} \tag{1.9}$$

Define mode Grüneisen parameter (which is treated as temperature independent itself) as

$$\gamma_{q,s} \equiv -\frac{V}{\omega(q,s)}\frac{\partial\omega(q,s)}{\partial V} \tag{1.10}$$

and inserting into the equation above we get

$$\alpha = \frac{K_T \sum_{q,s} \gamma_{q,s} C_{q,s}}{V} \tag{1.11}$$

With mean Grüneisen parameter defined as

$$\gamma = \frac{\sum_{q,s} \gamma_{q,s} C_{q,s}}{C_V}, \tag{1.12}$$

where $C_V = \sum_{q,s} C_{q,s}$ is specific heat of the structure within quasiharmonic approximation.

Thermal expansion coefficient is then related to isothermal compressibility K_T and constant volume heat capacity C_V by the Grüneisen formula:

$$\alpha = \frac{K_T \gamma C_V}{V} \tag{1.13}$$

Or in terms of bulk modulus of solids:

$$\alpha = \frac{\gamma C_V}{BV} \tag{1.14}$$

C_V as the heat capacity of a structure appearing in the nominator of (1.14) is proportional to the volume of the structure V which appears in the denominator, it is therefore better to represent $\frac{C_V}{V}$ as $\overline{c_V}$, which is specific heat of the structure per unit volume. And (1.14) is simplified into another form of Grüneisen formula:

$$\alpha = \frac{\gamma \overline{c_V}}{B} \tag{1.15}$$

Both bulk modulus B and specific heat $\overline{c_V}$ appearing in equation (1.15) are always positive dictated by fundamental thermodynamic laws; otherwise the structure would become unstable and self-exploding. The sign of thermal expansion α therefore is solely decided by average Grüneisen parameter of those vibration modes that are excited by temperature. Since the strength of interatomic interactions will decrease as interatomic distances increase, it is generally found that vibration frequencies in a structure tend to decrease in value as the volume increases, which means mode Grüneisen parameters $\gamma_{q,s}$ are usually positive

according to equation (1.10), leading to a positive mean Grüneisen parameter γ as in equation (1.12) which in turn decides a positive thermal expansion coefficient described by equation (1.15).

For materials with negative thermal expansion, clearly certain low energy "soft" modes (meaning low frequency) have unusually large negative mode Grüneisen parameters $\gamma_{q,s}$, and because these modes are low in energy relatively and dominating in (1.12), mean Grüneisen parameter becomes negative too, giving rise to a negative thermal expansion coefficient. Direct experimental evidence to single out these special vibration modes is still lacking, but their existence is predicted by lattice dynamic calculations as well as much indirect experimental evidence. These special vibration modes are the real makers of NTE!

The representation (1.15) also has two limiting forms, both with interesting practical implications. Since the bulk modulus appearing in the denominator of (1.15) is only weakly temperature-dependent, temperature dependence of thermal expansion coefficient is largely dependent on mean Grüneisen parameter γ and specific heat $\overline{c_V}$. As temperature approaches 0 K, only a very limited number of vibration modes would be excited and γ approaches a constant value implied by (1.12); if temperature is much higher than Debye temperature Θ_D, all vibration modes are thought as excited in Debye model and γ would approach another constant value though (1.12). In both extreme cases the temperature dependence of thermal expansion coefficient mainly comes from specific heat, i.e., it would be the

same as temperature dependence of specific heat in solids, which is well described by Debye model itself:

$$\alpha \sim T^3,\ T \to 0;$$
$$\alpha \sim constant, T >> \Theta_D. \tag{1.16}$$

Both limiting forms fit well with experimental measurements, and the second one is actually frequently observed in studying thermal expansion property of various oxide structure at high temperatures, where lattice parameters tend to increase or decrease (if we are lucky finding a NTE structure!) linearly with temperature, i.e., a constant thermal expansion coefficient, most often being positive, and a few times negative.

An interesting and open question arising from these two limiting cases related to NTE researches is that in the range where $\alpha \sim T^3$ at low temperature, could negative thermal expansion property of a structure be preserved? Or in other words, could NTE be preserved all the way up to 0 K until it becomes zero there (due to specific heat)? Nothing in the Grüneisen model appears to prevent such a possibility, yet to prove its existence could be a daunting task.

The Grüneisen model therefore provides the simplest theoretical framework within which thermal expansion property of solid oxides, both positive and negative, appears able to be satisfactorily explained. Applying the physical theory/model to real materials of various thermal expansion properties requires

identifying those special vibration modes with negative Grüneisen parameters that make the mean Grüneisen parameter of a structure negative. This appears to be far from a smooth and straightforward process, and so far a consensus has yet to be reached as to what vibration modes are really responsible for NTE in cubic α-ZrW_2O_8, the most studied structure being the best NTE material so far. It has been argued that only phonons of energy less than 10 meV are relevant to NTE in ZrW_2O_8 (25). Rigid unit modes (RUMs) corresponding to the correlated tilting and rocking motions of polyhedra relative to each other that exist in this structure have also been advanced as candidates for these NTE modes (26). Lattice dynamic calculations seem to suggest two transverse acoustic branches in the phonon spectrum are most responsible for NTE (27); and in high pressure Raman spectroscopic studies most optical modes below 50 meV are found to have negative Grüneisen parameter (28). Using the X-ray Absorption Fine Structure (XAFS) technique, modes that lead to NTE are proposed to correspond to the correlated vibrations of WO_2 tetrahedra and its three nearest ZrO_3 octahedra and involve vibrations along four equivalent <111> axes (20). For other NTE structures more detailed structure-property relationship studies by lattice dynamic methods have yet to start formally.

Among various experimental and computational methods used to study lattice dynamics of NTE materials as shown in the above, the most accessible one to us is lattice dynamic calculations, and its application to two NTE structures will be the topic of Chapter 5.

From a solid state chemist's perspective, a more relevant issue is probably how to bring results and understandings obtained in lattice dynamic studies of NTE materials, by both experimental and computational methods, back into the first line of material-structure work to aid new NTE material discovery, preparation and structure characterization. This appears to me part of a large unsolved problem in modern science of condensed phases, and the fact that we can differentiate two lines of work, one material-structure and the other structure-property, is exactly one symptom of the problem.

Since the question of which vibration modes in a structure are responsible for its NTE behavior is still open, it may be too early to attempt to relate these special NTE modes to any more simple and direct geometrical considerations or structure features, such as our working hypothesis that 2-coordinated oxygen atoms two polyhedra in a network structure using to share corners can induce negative thermal expansion. But this could be the direction we strive for to bridge the gap between new NTE material explorations and lattice dynamic theories, models, studies. One phenomenon might offer some clues here, which is the relationship, or rather correlation between phase transitions and negative thermal expansion.

It is not surprising that phase transitions are often encountered in studying thermal expansion behavior of oxide materials, since we study their structure changes over large temperature ranges, and phase transitions are bound to happen here and there. What is surprising is that there seems to exist certain correlation between (displacive) phase transitions and negative thermal expansion, of which

there are signs in four out of five networks we studied, such as ZrV_2O_7 in A_2MO_7 network, quartz in AO_2 network, $Sc_2W_3O_{12}$ in $A_3M_2O_{12}$ network and $NbOPO_4$ in AMO_5 network, while it is absent in MO_3 network, that also happens to show no obvious NTE. All phase transitions in these cases are more or less displacive phase transitions, and in the latter three examples structures show usual positive thermal expansion in lower temperature lower symmetry phases, which changes to unusual NTE above phase transitions in higher temperature higher symmetry phases.

According to lattice dynamic theory this observation might not be that surprising after all, since both displacive phase transitions and NTE share one common driving force: special vibration modes that lower their frequencies in special ways with increased temperature, often called soft modes in the standard model of displacive phase transitions. In a NTE structure their decrease in vibration frequency comes from changes in strength of interatomic interactions with respect to interatomic distances, when these modes become dominating they shrink the lattice; In a structure that undergoes a displacive phase transition these modes' frequencies decrease due to increased phonon-phonon interactions at higher temperature, and when the frequency of a soft mode becomes low enough to approach zero, it distorts the structure irreversibly and transfers it into another one.

But exactly how these two processes relate to each other on the microscopic level is not certain, some data analysis and tentative discussions on this subject are covered in Chapter 6.

1.5. References

1. G. Shirane and S. Hoshina, *J. Phys. Soc. Jpn.* 6, 265 (1951)

2. M. Blackman, *Philos. Mag.* 9, 831 (1958)

3. K. Röttger, A. Endriss, J. Ihringer, S. Doyle, and W.F. Khuss, *Acta Crystallogra.* Sect B 50, 644 (1994)

4. V. Korthius, N. Khosrovani, A. W. Sleight, N. Roberts, R. Dupree and W. W. Wareen Jr., *Chem.. Mater.*, 7, 412 (1995)

5. G. K. White, *Contemp. Phys.* 34, 193 (1993)

6. E. Bourova and P. Richet, *Geophysical Research Letters,* 13, 25, 2333 (1998)

7. P. Tschaufeser and S. C. Parker, *J. Phys. Chem..* 26, 99 (1995)

8. D. A. Woodcock, P. Lightfoot, L. A. Villaescusa, M. Diaz-Cabanas, M. A. Camblor, D. Engberg. *J. Mater. Chem.*, 349, 9 (1999)

9. T.A. Mary, J.S.O. Evans, A. W. Sleight and T. Vogt, *Science*, 272, 90 (1996)

10. Niangao Duan, A. W. Sleight etc, *J. Solid State Chem.*, 424, 139(1998)

11. Niangao Duan, A. W. Sleight etc, *J. Amer. Chem. Soc.*, 8694, 122(2000)

12. J.S.O. Evans, T.A. Mary and A.W. Sleight, *J. Solid State Chem.*, 137, 148 (1998)

13. P. M. Forster and A.W.Sleight, Inter. *J. Inorg. Mater.*, 1, 123 (1999)

14. P. M. Forster, A. Yokochi and A.W.Sleight, *J. Solid State Chem.*, 140(1), 157 (1998)

15. M. P. Attfield, A.W. Sleight, *Chem. Mater.*, 7, 10 (1998)

16. T. G. Amos, *Thesis* submitted to the Oregon State University, (2000)

17. H. M. Rieveld, *Acta Crystallogr.*, 151, 22 (1967)

18. A. Le Bail, H. Duroy and J.L. Fourquet, *Mat. res. Bull.* 447, 23 (1988)

19. W. R. Buessem, "Mechanical Propertiese of Engineering Ceramics", (W. W. Kreigel and H. Palmour III, Eds.), P. 127. Interscience, NY 1961

20. D. Cao, F. Bridges, G. R. Kowach, A. P. Ramirez, publication preprint

21. N. Khosrovani, A. W. Sleight, *J. Solid State Chem*, 2, 121 (1996)

22. K. D. Hammonds, M. T. Dove, A. P. Giddy, V. Heine, B. Winkler, *American Mineralogist*, 1057, 81 (1996)

23. N. W. Ashcroft and N. D. Mermin, "Solid State Physics", p. 492, Saunders College, 1976

24. M. T. Dove, "Introduction to Lattice Dynamics", p. 173, Cambridge University Press, 1993

25. G. Ernst, C. Broholm, G. R. Kowach, and A. P. Ramirez, Nature (London) 396, 147 (1998)

26. A. K. Pryde, K. D. Hammonds, M. T. Dove, V. Heine, J. D. Gale, M. C. Warren, *J. Phys.: Condens. Matter* , 8 (1996)

27. R. Mittal and S. L. Chaplot, *Phys. Rev. B* 60 (1999)

28. T. R. Ravindran, A. K. Aroura, T. A. Mary, *Phys. Rev. Letters*, 17, 84 (2000)

Chapter 2

Thermal Expansion Study of MO_3 Type Structure: $(Ta/Nb)O_2F$

2.1. Introduction

Frevel and Rinn first reported synthesis and structure characterization of NbO_2F and TaO_2F in 1956 (1). The powder diffraction patterns obtained could be indexed on the basis of a primitive cubic cell, and the powder of tantalum dioxyfluoride was found to be isotropic under a polarizing microscope. Comparing the powder pattern of TaO_2F with that of $TiOF_2$ (2) immediately suggested that they are isostructural with ReO_3, a 3-D network of interconnecting corner-sharing cation-anion octahedra that are ideal. Relative intensities measured photographically compared favorably with integrated intensities based on a ReO_3 structure. TaO_2F was also found to decompose above 500 °C into Ta_2O_5.

2.2. Experimental

Powder crystalline samples of NbO_2F and TaO_2F were prepared following the method by Frevel and Rinn (1): weighted amount of metal powder (99.9%) was

dissolved in 48% concentrated HF solution in a platinum crucible at about 80 °C. The clear colorless solution was then evaporated to dryness and resulted white residual was heated around 450 °C for about 5 hours to obtain a white powder. Samples were further annealed around 300 °C for about 48 hours before powder diffraction data collection or pressed into pellets for dilatometer measurements.

The bulk thermal expansion was measured with a Netzsch STA 409 dilatometer using sapphire as internal standard and fused silica was used to calibrate the instrument. A sample bar sintered overnight at 300 °C with approximate dimension of 25×5×5 mm was heated at a rate of 10 °C/minute from room temperature to 500 °C.

Low temperature powder diffraction data were collected from 20 K to 300 K at 0.700418 Å on the beam line x7a of the National Synchrotron Light Source (NSLS) at the Brookhaven National Lab. A small amount of well ground fine powder samples were filled into and sealed in 0.2 mm caliber capillaries and mounted into a liquid nitrogen cooled thermostat. The beam line x7a diffractometer collects diffraction data with a small position sensitive detector (PSD) in transmission mode. Powder diffraction data from 200 K to 400 K were collected on an Inel 590 multipurpose powder diffractometer equipped with a 90 degree position sensitive detector and a cryostat in transmission mode; those from 300 K to 773 K were collected on the same diffractometer in reflection mode with a customized furnace.

2.3. Thermal Analysis

A change in the bulk thermal expansion was observed for both NbO_2F and TaO_2F (Figure 2.1). For NbO_2F it shows a positive thermal expansion from room temperature to about 175 °C, then a negative thermal expansion up to 500 °C with an estimated thermal expansion coefficient of -6.0×10^{-5} /K. The same kind of trend is observed for TaO_2F.

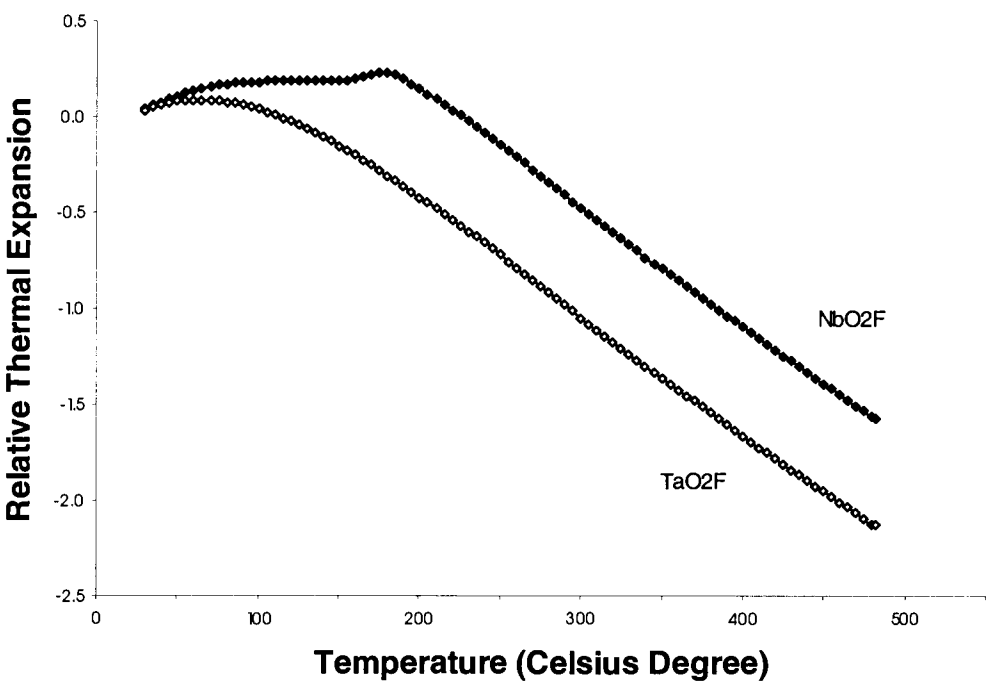

Figure 2.1. Dilotometry measurement of bulk thermal expansion of $(Ta/Nb)O_2F$

2.4. Structure Refinement

The structures of both NbO_2F and TaO_2F are ReO_3 type consisting of a corner sharing network of ideal Nb/Ta-O/F octahedra. There is a single cation on the (0, 0, 0) site and 2 oxygen atoms and one fluorine atom completely disordered at (0, 0, ½). Each octahedron shares all six corners with adjacent octahedra and the whole structure has the symmetry of space group *Pm3m*. A ball-and-stick representation of the structure is illustrated in Figure 2.2.

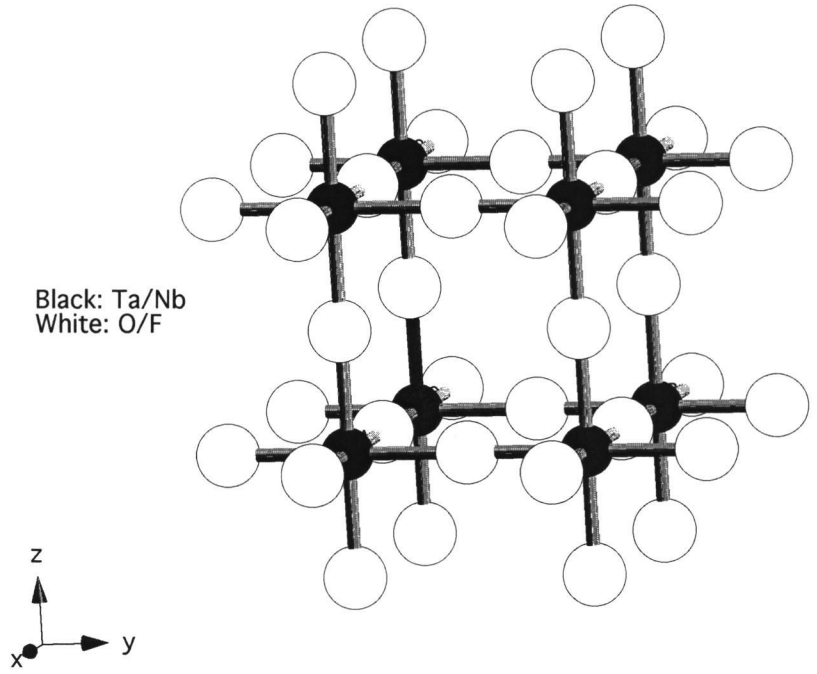

Figure 2.2. Structure of TaO_2F and NbO_2F.

Powder diffraction data collected over all the temperature ranges were used to refine the structure of NbO_2F and TaO_2F though GSAS suite of programs (3). There is only one structure parameter that is not fixed by the space group *Pm3m*, i.e., cubic lattice parameter *a*, its initial starting value is adopted from that reported by Frevel and Rinn (1). A total of 14 parameters (1 zero point, 1 scale parameter, 3 background parameters, 6 profile parameters {GU, GV, GW, LX, LY, asym}, 1 lattice parameter, 2 thermal displacement parameters) were refined in Rietveld runs, and 11 parameters excluding scale parameter plus two thermal factors for Le Bail runs.

Table 2.1 lists the refinement statistics of synchrotron TaO_2F data, and Figure 2.3 shows the agreement between the observed and calculated intensities for a typical rietveld refinement run.

Table 2.1. Refinement statistics of TaO_2F synchrotron powder diffraction data

Temperature (K)	χ^2	wRp	Rp
20	*6.515*	*0.0986*	*0.0937*
50	*6.243*	*0.1008*	*0.0938*
100	*5.836*	*0.1024*	*0.0902*
150	*6.483*	*0.1051*	*0.0952*
200	*6.677*	*0.0887*	*0.0827*
250	*6.054*	*0.0901*	*0.0846*
300	*5.448*	*0.0895*	*0.0831*

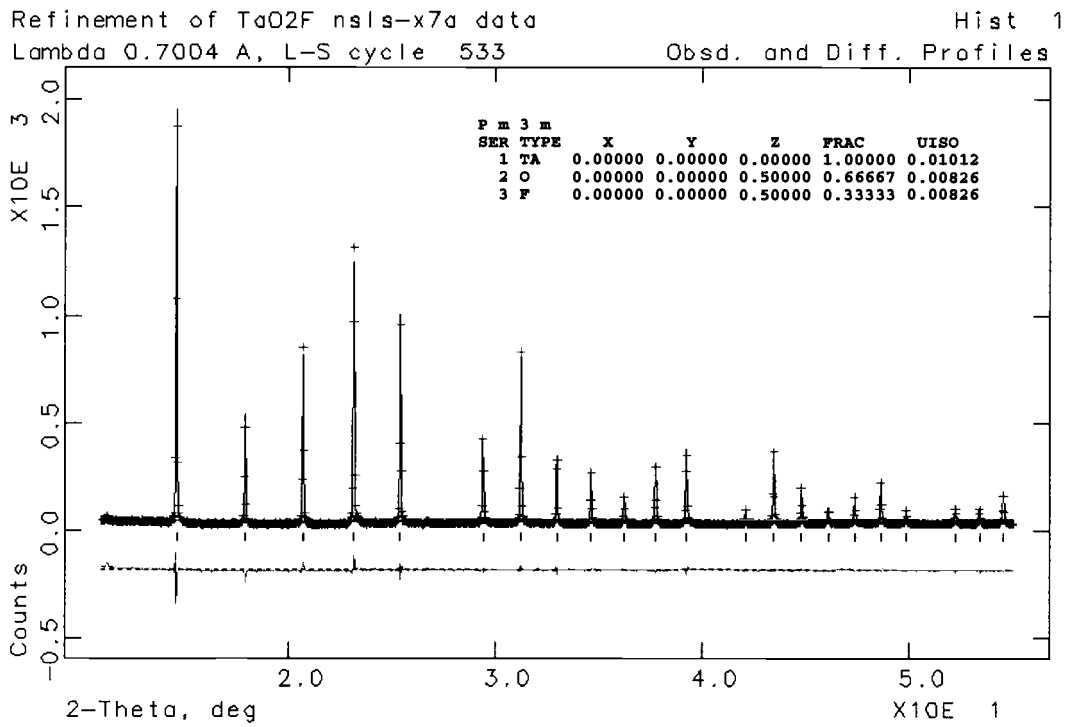

Figure 2.3. Observed (+), calculated (line) and difference (lower line) synchrotron diffraction patterns for TaO_2F at 20 K. Lower tick marks represent calculated Brag peak positions.

Structure refinements of synchrotron data indicate TaO_2F has very small thermal expansion coefficient from 25 K to 773 K, no larger than $\pm 1.5 \times 10^{-6}$ /K by estimate, NbO_2F has a positive thermal expansion (up until room temperature). The change of cubic cell parameters as function of temperature is plotted in Figure 2.4.

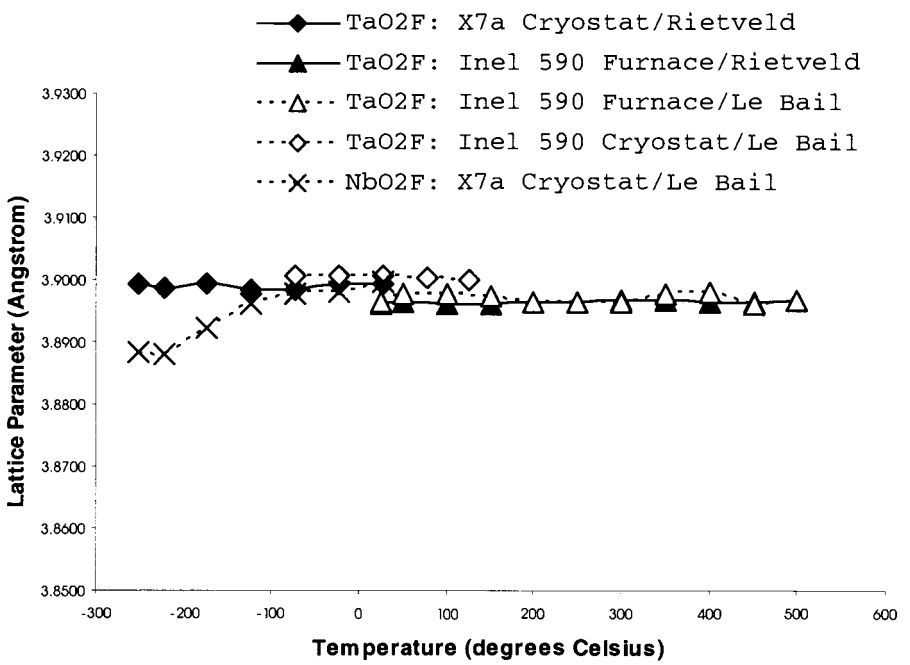

Figure 2.4. Lattice parameters of TaO_2F and NbO_2F as a function of temperature

2.5. Discussion

Because of small magnitudes of both thermal expansion coefficient and lattice parameter of TaO_2F itself, the change of lattice parameters from thermal expansion appear to be very small in this material, its value comparable to errors in cell parameter values due to instrumentation, data collection and structure refinement methods themselves. As a result the value of the lattice parameter as a function of temperature oscillates within a very narrow range of ±0.001 Å 27 K to 300 K instead of being a smooth (positive or negative) expansion curve with a clearly identifiable trend line. The best we can conclude is that TaO_2F has a very low thermal expansion in the temperature range, whether it is positive or negative is still uncertain.

One important source of these systematic errors is the asymmetry of diffraction peaks, which has its origin in both limitations of diffratometer instrumentation and crystal structures being nonideal, with the latter usually more important but convoluted with instrumentation errors. The way the Rietveld method or whole pattern fitting Le Bail method handles asymmetry is by adding a small correction term to usual symmetrical profile functions (peak broadening functions) such as Pseudo-Voigt function, which is the product of a small empirical parameter ("asym" in GSAS program) between 0 and 1 and first derivatives of symmetrical profile functions. Clearly the procedure is purely empirical and introduces errors to final refined structure parameters.

This error is clearly present for synchrotron TaO_2F data and appears to be a major one. Table 2.2 compares final lattice parameter values from structure refinement of synchrotron TaO_2F data with symmetrical pseudo-voigt profile function and its corresponding asymmetrical form.

Table 2.2. Comparison of refined lattice parameter values using symmetrical profile functions with those using asymmetrical profile functions.

Profile Function:	Asymmetrical	Symmetrical
Temperature (K)	Lattice Parameters (Å)	
20	*3.8995*	*3.8983*
50	*3.8986*	*3.8983*
100	*3.8992*	*3.8980*
150	*3.8984*	*3.8972*
200	*3.8982*	*3.8970*
250	*3.8993*	*3.8981*
300	*3.8994*	*3.8981*

For the purpose of a qualitative assessment of systematic errors in lattice parameter values, the dependence of the mean square thermal displacement on temperature for TaO_2F is plotted in Figure 2.5. In the high temperature classical limit this quantity should increase linearly with temperature, and for both Ta and O/F atoms it appears as an overall trend indeed, which implies overall structure refinement quality is acceptable. At the same time large deviations of its values from an ideal straight line suggest the existence of many systematic errors, which are usually picked up by thermal displacement parameters, one reason being that they are often the last structure parameters to be refined.

That the slope of oxygen/fluorine line is larger than that of tantalum line is as expected, since O/F has a smaller mass and their thermal displacement should increase faster with temperature. Ta atoms having larger thermal displacement than O/F at lower temperature is, however, a little unusual for the same reason. It could be related to the same type of structural defects as reported in (4).

Another unresolved issue is the discrepancy in thermal expansion behavior between that which was observed through direct dilatometry measurements (Figure 2.1) and values obtained by diffraction methods (Figure 2.4). The latter should be more reliable, and large instrumental or systematic errors in dilatometry measurements could produce a misleadingly thermal contracting curve as shown in Figure 2.1. However, the possibility of an extrinsic type of negative thermal expansion, even when both TaO_2F and NbO_2F are cubic, can't be totally ruled out.

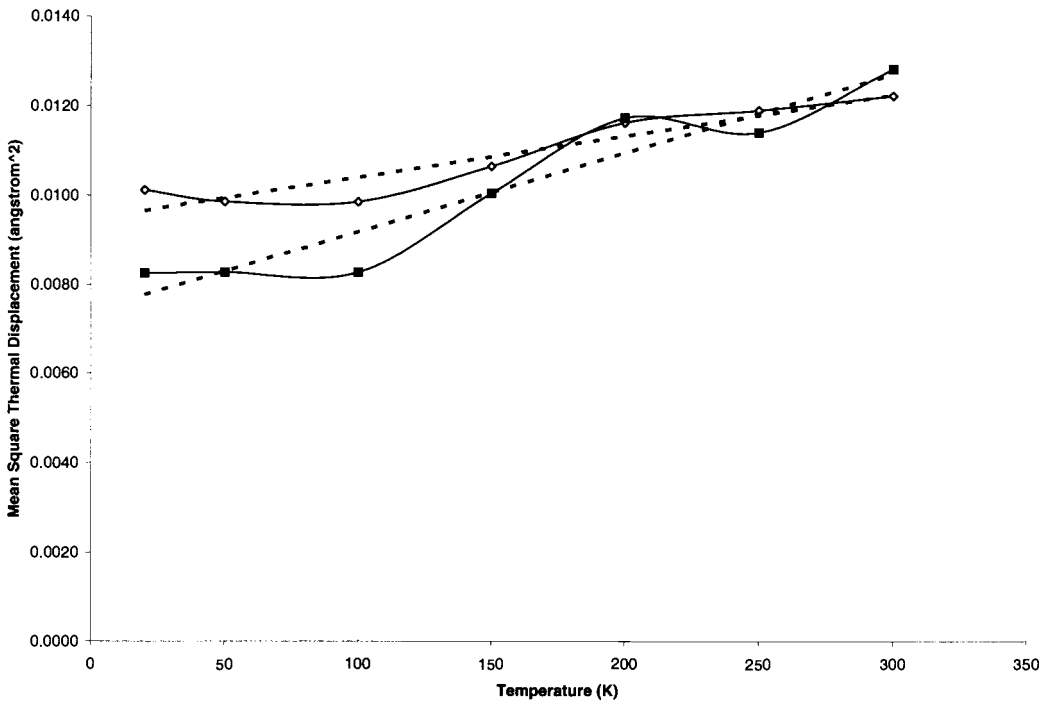

Figure 2.5. Dependence of atom mean square thermal displacements on temperature

2.6. References

1. L. K. Frevel and H. W. Rinn, *Acta Cryst.*, 626, 9 (1956)

2. K. Voores and J. Donohue, *Acta Cryst.*, 25, 8 (1955)

3. A. C. Larson and R. B. Von Dreele, LANSCE, Los Alamos National Lab, Los Alamos, NM, 1994

4. S. Andersson, *Acta Chem. Scand.*, 2233, 18 (1964)

Chapter 3

Introduction to Computation Methods

3.1. Thermal Expansion Coefficient

From a theoretical or computational point of view, studying negative thermal expansion property of a material is ultimately reduced to calculating the thermal expansion coefficient of its idealized structure, usually at (and referring to) ambient pressure (1 atmosphere). This is defined as:

$$\alpha = \frac{1}{V}\left(\frac{\partial V}{\partial T}\right)_p$$

where α is a structure's (volumetric) thermal expansion coefficient, V its volume (lattice parameters for crystalline structures), T temperature and P pressure. If direct calculations are impractical, one can attempt to relate a material's thermal expansion property to certain higher level structure features that are more accessible by computational or modeling approaches.

Excluding phase transitions which introduce discontinuities into crystal structures, thermal expansion is essentially a very small perturbation of the ideal crystal structures at 0 K. For typical unit cells with a dimension 3~10 Å, the root-

mean-square atomic displacement due to thermal vibrations has a typical order of magnitude about 0.3 Å (1) at room temperature, and is proportional to square root of temperature in high temperature classical limit. Thermal expansion of the lattice is a higher order effect of this atomic vibration motion or perturbation, with typical values having an order of magnitude no larger than 0.01 Å. It is for this reason that thermal expansion coefficients of crystalline materials have values in a very small range, typically between $\pm 10^{-5}$ /K.

From a solid state chemist's perspective, exact values of thermal expansion coefficients for any given crystal structure are decided by its geometric crystallographic features, namely network topography in terms of 3-D connectivity of metal oxygen polyhedra, crystal symmetry in terms of a specific space group and chemical bonding in terms of individual atom positions in a unit cell, and by all kinds of forces in existence in the structure, usually parameterized as different (local) interatomic potentials based on a given geometric framework. If the "combination" of "geometry" and "force" halves is "right" for a certain structure, its thermal expansion coefficient would be smaller than zero, giving rise to interesting as well as potentially useful negative thermal expansion property.

However, direct calculation of thermal expansion coefficients, or lattice parameter change with respect to temperature, is not practical in most cases, due to incomplete knowledge of interatomic forces in a structure (lack of proper interatomic potential models and parameters) in lattice dynamic methods, or computation complexity as well as cost in higher level calculations. It is also

unnecessary in most cases, since the majority of materials have their thermal expansion coefficient within a very narrow range (from 10^{-6}/K to 10^{-5}/K, plus or minus), and the sign is far more important than exact values. It has been one motivation of this thesis work to look for a model or method that could predict the signs of thermal expansion (coefficient) of a crystalline structure relatively easily and reliably. The results are largely negative in this aspect and point to the tentative conclusion that this kind of model or method is probably unattainable at all (next chapter). However, direct calculations of the thermal expansion property based on one (semi-classic) lattice dynamic method are successful.

3.2. Different Models and Methods

Between two kinds of factors that decide a structure's thermal expansion property, the "structural/geometry" part being a material's normal crystallographic information (space groups, lattice parameters and atom positions) is readily available from literature, or relatively easy to determinate, and always included in any models or methods treating thermal expansion properties. The 'force' part, namely all the interatomic interactions within a structure, is a more demanding one: in one end of the spectrum there are quantum mechanical methods that treat these forces in an *ab initio* way, reducing them to nothing more than atomic numbers and many interacting quantum mechanical equations, which is typical of condensed

matter physicists' approaches, also typical of its restrictions and limitations and beyond the scope of this thesis work; in the other end we can neglect this part completely and emphasize how thermal expansion of a structure relates to its geometry parameterized in terms of metal-oxygen polyhedral and interatomic bond distances, the Distance Least Square (DLS) method exemplified by Nazi and Sleight (2). In between these two methodic extremes there are two intermediates: one that allows certain harmonic forces acting between metal-polyhedron, the Rigid Unit Mode model (3) discussed in more detail in next chapter; the other approximates these interatomic interactions with well known shell model interatomic potentials and apply quasiharmonic approximation to the problem (4), the lattice dynamic free energy minimization method. Its results are presented in next next chapter. While DLS method and RUM method in most cases take into account only geometry parameters and no forces so it could be called 'zero' order, free energy minimization within quasiharmonic approximation corresponds to first order approximation in quantum mechanic perturbation treatments.

3.2.1. Rigid Unit Mode (RUM) model and method

In the RUM model all interatomic forces within a structure being assumed to be harmonic or nonexistent, the immediate consequence is that thermal expansion, one of most common anharmonic effects, would be always zero in such a model. The

value of this method therefore doesn't come from any numerical evaluation of thermal expansion coefficient values, but from the fact that a structure with harmonic interactions is very simple, and its phonon structure could be easily calculated. It was proposed certain special vibration modes in this spectrum (they have zero calculated vibrational frequencies and are called rigid unit modes) are the underlying mechanism for negative thermal expansion property (5).

The potential energy in quasiharmonic approximation is a quadratic form:

$$U = \frac{1}{2} \sum_{ss';ll';jj'} G^{jj'}_{sl;s'l'} u^{j}_{sl} u^{j'}_{s'l'} \tag{3.1}$$

Each G is Fourier transformed to:

$$D^{jj'}_{ss'}(\mathbf{q}) \equiv \sum_{\mathbf{h}} \mathbf{G}^{\mathbf{jj'}}_{\mathbf{sl;s'l'}}(\mathbf{h}) \mathbf{e}^{\mathbf{iq\cdot h}} \tag{3.2}$$

where $\mathbf{q} = \zeta \mathbf{a}^* + \eta \mathbf{b}^*$ is a wave-vector in reciprocal space, $\mathbf{h} = \mathbf{l}' - \mathbf{l}$ is a translational vector in real space.

$D^{jj'}_{ss'}$ is the $3n \times 3n$ dynamic matrix, solving the eigenvalue problem of this matrix we find vibration frequencies (eigenvalues) and normal modes (eigenvectors). RUMs are vibration modes with $\omega = 0$.

For the 2-D tile network as illustrated in Figure 2.1 (6), Hamitonian is:

$$
\begin{aligned}
H &= \tfrac{1}{2}\sum_{m,n}\left(\dot{x}_{m,n}^2+\dot{y}_{m,n}^2+a^2\dot{\theta}_{m,n}^2\right)\\
&+\tfrac{K}{2}\sum_{m,n}[(x_{m,n}-x_{m+1,n})^2+(x_{m,n}-x_{m,n+1})^2\\
&+(y_{m,n}-y_{m+1,n})^2+(y_{m,n}-y_{m,n+1})^2\\
&+\tfrac{a^2}{4}(\theta_{m,n}+\theta_{m+1,n})^2+\tfrac{a^2}{4}(\theta_{m,n}+\theta_{m,n+1})^2\\
&+a(y_{m,n}-y_{m+1,n})(\theta_{m,n}+\theta_{m+1,n})-a(x_{m,n}-y_{m,n+1})(\theta_{m,n}+\theta_{m,n+1})]
\end{aligned}
\tag{3.3}
$$

For $G_{sl;s'l'}^{jj'}$ in equation (3.2),

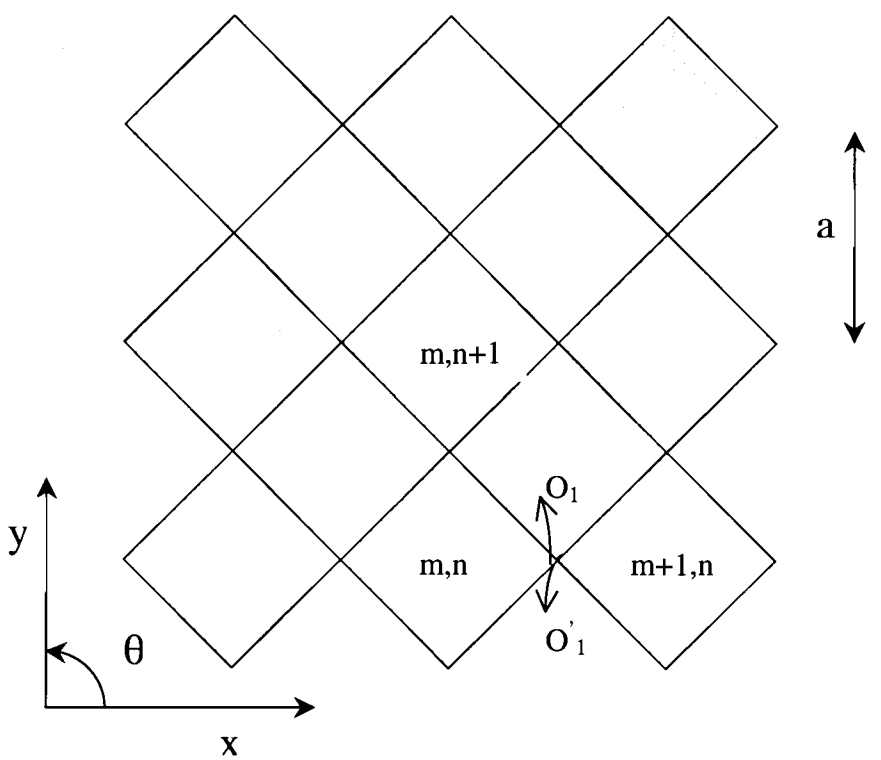

Figure 2.6. A 2-D tile network

$s = s' = 1,\ j(j') = x, y, \theta$

And

$(l, l') \in \{(m,n;m,n),(m,n;m+1,n),(m,n;m-1,n),(m,n;m,n+1),(m,n;m,n-1)\}.$

With Hamitonian available we can find out G, then Fourier transform it to get dynamic matrix D. Taking D^{xx} as an example:

x^2 term in the Hamitonian is:

$$2x_{m,n}^2 + x_{m+1,n}^2 + x_{m,n+1}^2 - 2x_{m,n}x_{m+1,n} - 2x_{m,n}x_{m,n+1}$$

with m and n being indices for the sum, therefore

$$G^{xx}_{m,n;m,n} = 4$$

$$G^{xx}_{m,n,;m-1,n} = -1$$

$$G^{xx}_{m,n,;m+1,n} = -1$$

$$G^{xx}_{m,n,;m,n-1} = -1$$

$$G^{xx}_{m,n,;m,n+1} = -1$$

$$D^{xx} = 4 - e^{-2i\pi\zeta} - e^{2i\pi\zeta} - e^{-2i\pi\eta} - e^{2i\pi\eta} = 4 - 2[\cos(2\pi\zeta) + \cos(2\pi\eta)]$$

The same procedure could be carried out for each element of the dynamic matrix and it turns out to be:

$$\begin{pmatrix} 4K(1-\alpha) & 0 & -\gamma K \\ 0 & 4K(1-\alpha) & \beta K \\ \gamma K & -\beta K & ka^2(1+\alpha) \end{pmatrix}$$

with

$$\alpha = \frac{1}{2}[\cos(2\pi\zeta) + \cos(2\pi\eta)]$$
$$\beta = ia\sin(2\pi\zeta)$$
$$\gamma = ia\sin(2\pi\eta)$$

Only with two wave-vectors eigenvalues $\omega(q) = 0$ for this dynamic matrix:

$q = (0,0)(\alpha = 1, \beta = \gamma = 0)$,

a trivial solution corresponding to translation of the whole lattice;

$q = (0.5,0.5)(\alpha = -1, \beta = \gamma = 0)$,

with eigenvector $(0,0,1)$,This is the RUM that only involves tilting of tiles along $\hat{\theta}$, the rigid unit mode for 2-d tile network structure.

3.2.2. Free Energy Minimization with Quasiharmonic Approximation

From a thermodynamic point of view, thermal expansion could be interpreted as a structure's response to changing temperature to keep its (Gibbs) free energy minimized, as required by the second law of thermodynamics. The problem of calculating volume (unit cell parameters) of a structure at a specific temperature therefore is converted to finding the volumetric value that minimizes its free energy, and repeating this procedure at different temperatures values. The energy part of free energy evaluation is obtained by setting up parameterized interatomic potentials and summing them up at equilibrium distances; the contribution from vibration entropy is calculated by sampling at various points in Brillouin Zone. To make computations analytically possible, this procedure is carried out under the quasiharmonic approximation, which assumes thermal vibration frequencies change with cell volumes at different temperatures, but other than that they are totally harmonic.

3.3. References

1. M. T. Dove, "Introduction to Lattice Dynamics", p. 61. Cambridge University Press, 1993

2. N. Khosrovani, A. W. Sleight, *J. Solid State Chem*, 2, 121 (1996)

3. K. D. Hammonds, M. T. Dove, A. P. Giddy, V. Heine, B. Winkler, *American Mineralogist*, 1057, 81 (1996)

4. N. W. Ashcroft and N. D. Mermin, "Solid State Physics", p. 492, Saunders College, 1976

5. A. K. Pryde, K. D. Hammonds, M. T. Dove, V. Heine, J. D. Gale, M. C. Warren, *J. Phys.: Condens. Matter* , 8 (1996)

6. A. P. Giddy, M. T. Dove, G. S. Pawley and V. Heine, *Acta, Cryst.* 697, 49(1993)

Chapter 4

Rigid Unit Mode Model and Method

4.1. Introduction

The Rigid Unit Mode (RUM) model is developed from work that studies crystallographic structures, phase transitions and physical properties of framework silicates (1). It has long been recognized that existence of Si-O tetrahedra is the most conspicuous structure feature in this type of solid materials: they are geometrically ideal with four equal length Si-O bonds spaced symmetrically away from each other; adequately rigid to be common building block in all kinds of 3-D networks; and very stable across phase transitions to retain its shape and size. Later lattice dynamic studies of quartz drew attention to the fact that soft modes of displasive phase transitions in these structures should also involve the tetrahedra moving as rigid units, since dynamic atomic motions associated with the soft mode correspond to static displacements associated with this kind of phase transitions. Soon it was realized that the idea of lattice vibrations in which SiO_4 tetrahedra move as rigid units have important quantitative as well as property implications, and a modeling method to generalize the idea is developed by (2), implemented through a computer program CRUSH (3).

In this Rigid Unit Model (RUM) a framework structure is viewed as a 3-D periodic network of interconnecting metal-oxygen polyhedron, which are treated as rigid units, a classic mechanical structure with a mass, a moment of inertia, three translational degrees of freedom, and three vibration degrees of freedom. No other forces or interactions exist between these rigid units except the rigid connectivity between neighboring connected ones. Vibration waves supported by this kind of idealized network structures are called Rigid Unit Modes (RUMs).

After publication of the work on negative thermal expansion property of ZrW_2O_8 (4) through a large temperature range that has drawn fair amount of attention to thermal expansion study of framework oxides, Dove (5) first applied the RUM method to ZrW_2O_8, in which structure a surprisingly large amount of rigid unit modes were found; later computational and experimental studies in framework silicates also discovered possible signs of correlation between a structure's negative thermal expansion property and the existence of rigid unit modes within it. This chapter presents the work and results in studying negative thermal expansion property of all types of framework oxides by RUM method.

4.2. Some Notes on the Calculation of RUM

The RUM method is implemented computationally by the split-atom method (3), where a structure is viewed as a 3-D network of independent polyhedron

"molecules", and each O atom that is shared by two linked polyhedra is considered to be two individual "atoms" separated by a distance of zero. To prevent split atoms from separating, a strong harmonic force acts between them. The dynamic equations of this structure are then solved using standard procedures for the calculation of phonon dispersion curves for molecular crystals (as shown by the 2-D tile network example in the last chapter), and RUMs are calculated to be normal modes with zero frequency, since split halves behave like one single unit in these modes, which is what we would expect in a real structure where atoms are not "split". A computer program called CRUSH is designed to implement this procedure.

CRUSH takes as input a structure's lattice parameter and individual polyhedral positions (coordinates of its component atoms), and calculates normal mode coordinates and frequencies at specified points in the Brillouin zone (wavevectors). Searching for RUMs in a structure is carried out by providing a list of points in a symmetry reduced Brillouin zone (usually with 0.01 increment), and all modes with frequencies below certain criterion (usually 0.0001 cm^{-1}) are considered as RUMs (due to floating point errors this problem is always existent, but RUMs usually appear continuously in branches with higher symmetry throughout the Brillouin zone, making the problem nonimportant). Mathematical formalism of the RUM method is discussed in the last chapter, a general procedure for RUM modeling is outlined in Figure 4.1, a typical input file is shown in Figure 4.2. Common RUM runs take about 2 days to 1 week to complete, largely depending on the number of

polyhedra in a unit cell and the number of K points in the Brillouin Zone where RUMs are calculated/searched.

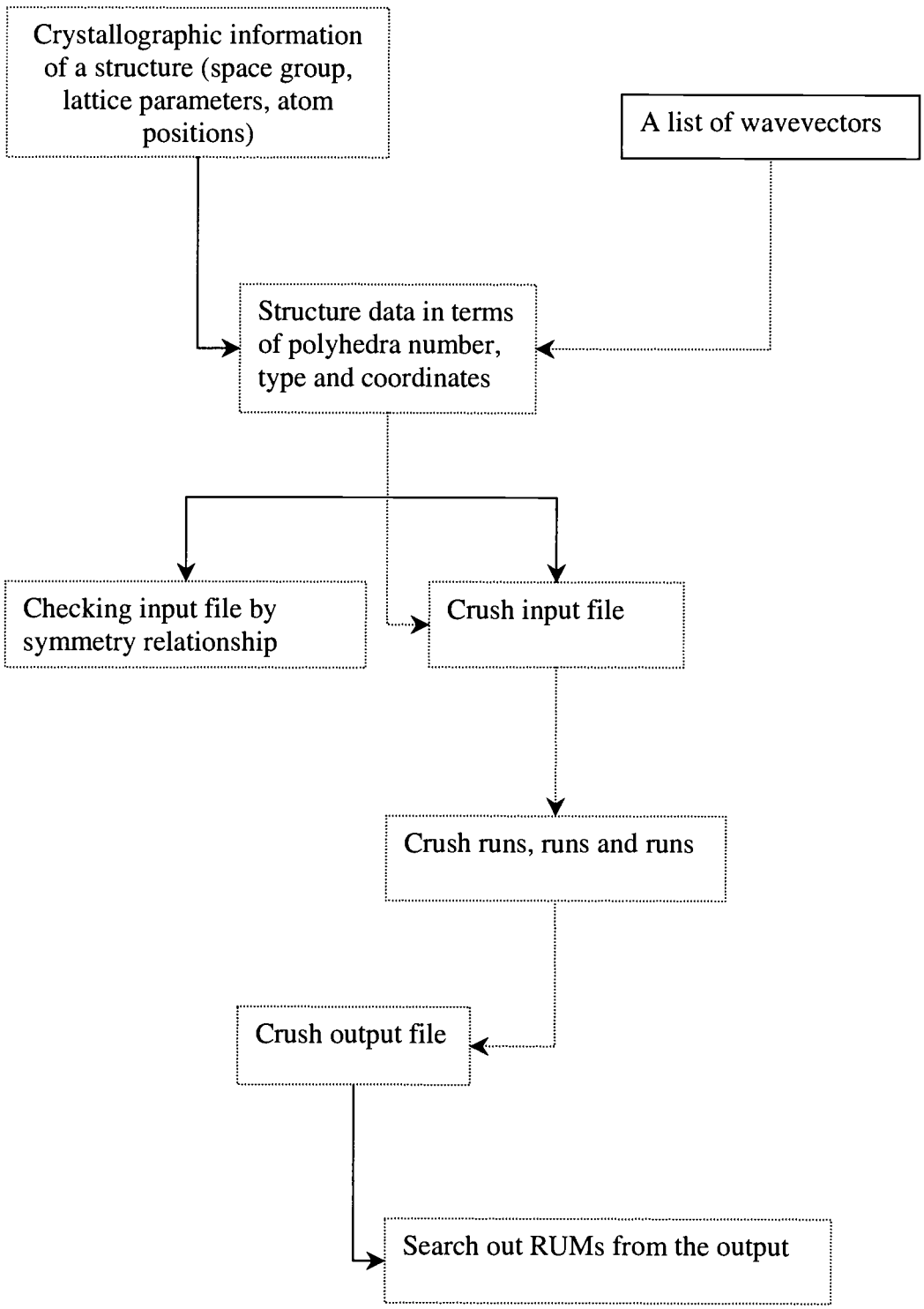

Figure 4.1. A general procedure for RUM modeling using program CRUSH.

```
Title line : AlPO4-17 run 1, P63/m, 100*100*100
27 Cells interact with the central one
177534.  0. Spring constants
3 Different atoms in structure
16.00 Mass of atom 1 oxygen
30.97 Mass of atom 2 Phosphorus
26.98 Mass of atom 3 Aluminum
F    "T": Average the moments of inertia of each rigid unit
F 0 F "T": fort.3 for ANALYSE; # of eigenvectors output to fort.11
(zero for no output); T: ASCII
0    the number of eigenvectors wanted in the formatted file fort.8
1 T  the number of frequencies in fort.8; T: cm-1 unit
F F  "T": eigenvectors in fort.8 in magnitude/phase angle format; T:
phase factor e^(i*k*r) removed
F    "T": participation coefficients output to fort.1
0    If 1-8 then neutron scattering calculations are performed.
-1 1 -2 3 0 1 are the hkl plane lower and upper limits for the above.
36   Number of rigid units in primitive unit cell.
5 5 5 5 5 5 5 5 5 5 5 5 5 5 5 5 5 5 5 5 5 5 5 5 5 5 5 5 5 5 5 5 5 # atoms
13.89787 13.89787 15.3302 90.00000 90.00000 120.00000 cell constants
0.  0.  0.  Cells arranged around the central cell at these fractional coordinates.
1.  0.  0.
...
-1 -1 -1 (27 neighbouring cells)
.2405 .0022 .1012 2
.325 .98 .1575 1
.1089 .908 .114 1
 2544 .1214 .1261 1
.2774 .003 .005 1
...
.9978 .2383 .1012 2
.02 -.655 .1575 1
.092 -.7991 .114 1
.8786 .133 .1261 1
.997 .2744 .005 1  (for all 36 polyhedra)
.0 .0 .0 { $Gamma$ point.}
0.1 0.2 0.3
0.9 0.8 0.7
99. .0 .0 {end of wavevector list}
```

Figure 4.2. A typical CRUSH input file.

Because in general polarization vectors of lattice waves are not real, and each rigid unit (polyhedron) has 6 degrees of freedom (three rotational ones are really hard to project and visualize), real space pictures of RUM motions are almost impossible to produce. Only in a few extreme cases they could be visualized as in the ideal MO_3 octahedra corner-sharing network (Section 4.7), where RUM motions are reduced to the type of "rocking motions" widely used in studying perovskite type framework structures.

4.3. Different Types of Framework Oxides and Their RUM Calculations

As discussed in Chapter 1 there are five families of oxide materials that have been explored and studied for their thermal expansion properties: AO_2, A_2MO_7, $A_3M_2O_{12}$, AMO_5, and MO_3, with ZrW_2O_8 viewed as a special case of A_2MO_7 type. These are also five types of framework structures which have been studied by RUM modeling with an eye toward their negative thermal expansion properties.

4.4. AO_2 Network

All structure types in the literature called framework silicates fall into this category, and with respect to negative thermal expansion properties it is also best

studied next to ZrW_2O_8, both experimentally and computationally. Among hundreds of types of different AO_2 networks and thousands of kinds of various structures and chemical compositions, there is a growing number of them that are shown to possess the negative thermal expansion property by quantitative temperature varying diffraction studies. But these NTE silicates and aluminophosphates still remain as exceptions, and no common structure features could be identified to separate them out as a group within framework silicates, except NTE itself. Since interatomic interactions operating within and through a structure, namely the 'force' part of factors that affect thermal expansion coefficients, are more or less the same for all framework silicates, therefore we can't simply attribute their differences in thermal expansion behavior, most assumed to be positive while a few are negative, to straight geometric reasons.

This reasoning suggests underlying mechanisms responsible for negative thermal expansion is neither pure structural and geometrical, i.e., a right set of bond distances and angles, nor only due to right kinds of interatomic interactions or "forces". Rigid Unit Modes, which is a common and important feature among framework silicates bridging between geometric structures and ineratomic forces, have been considered as a possible candidate to the mechanism underlying NTE, but extensive RUM calculations done within this thesis work negate a simple and direct correlation.

4.4.1. Structures with Both RUM and NTE

The aluminophosphate, $AlPO_4$-17, is comprised of alternating, corner-sharing AlO_2 and PO_2 tetrahedra (figure 4.1), the negative thermal expansion property of this material has been predicted from the results of computer simulation, and further determined experimentally. It is shown to have an unusually large negative thermal expansion coefficient (-11.7×10^{-6} /K over the temperature range 18-300 K) (6).

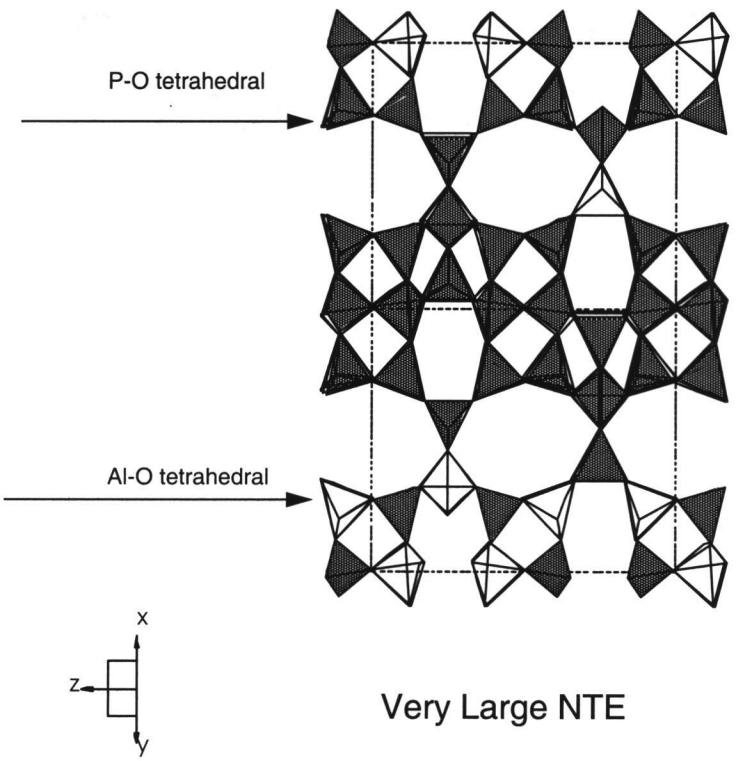

Figure 4.3. $AlPO_4$-17 structure consists of corner sharing AlO_2 and PO_2 tetrahedra.

The structure has very high six fold symmetry of space group $P6_3/m$, which decides the symmetry of (the first) Brillouin Zone to be 6/m (C_{6h}), the point group of this space group (176). Figure 4.4 shows how the symmetry reduced Brillouin Zone (shaded area) is determined, which is used to generate a list of symmetry irreducible K points to search out RUMs in this structure as described in the following:

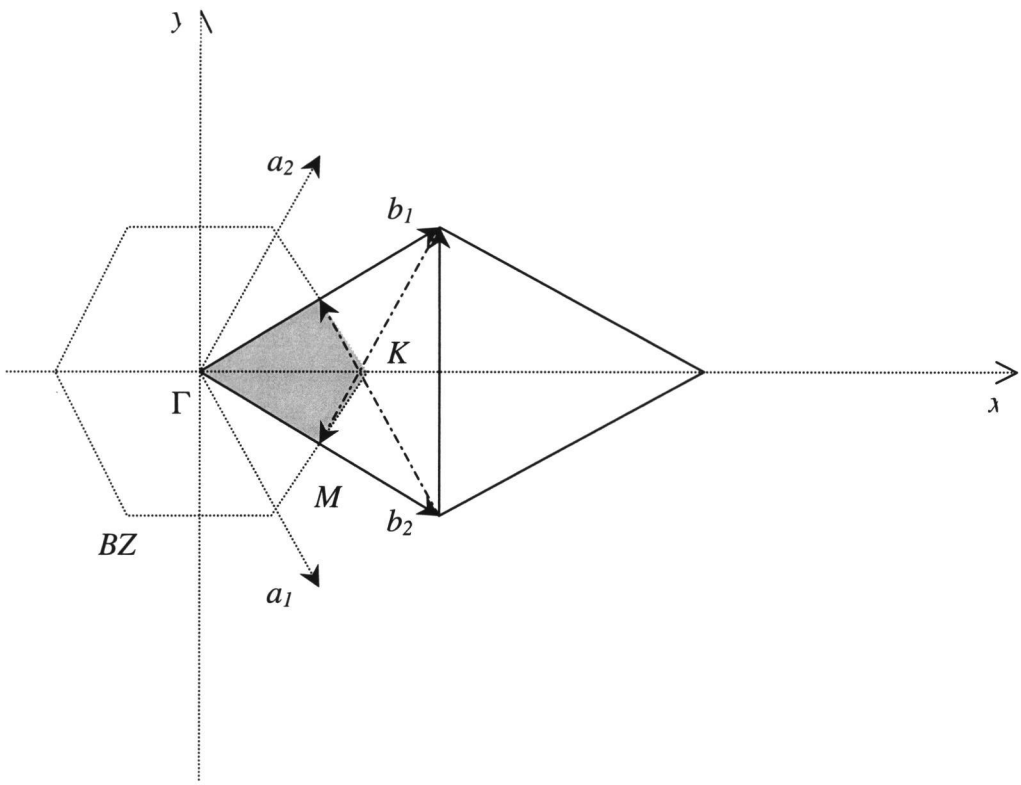

Figure 4.4. Symmetry reduced Brillouin Zone (shaded area) in a hexagonal lattice viewed down (0, 0, 1).

First a 3-D grid of K points is generated in the (first) Brillouin Zone:

$$\bar{k} = \frac{l}{100}\bar{b}_1 + \frac{m}{100}\bar{b}_2 + \frac{n}{100}\bar{b}_3 \text{ with } l=0..50,\ m=0..50,\ n=0..50$$

Those points with *l* and m larger than 50 are obviously outside the shaded area and therefore equivalent to some points inside through various symmetry operations; points with *n* larger than 50 are equivalent to points with *n* smaller than 50 by the mirror plane symmetry operation in 6/m point group. Therefore only K points within the volume defined by wavevectors *(0.5, 0, 0), (0, 0.5, 0)* and *(0, 0, 0.5)* are considered.

Next K points with their X-Y projections falling out of the shaded area were further sifted out to generate a list of wavevectors that distribute uniformly in the Brillouin Zone and are also symmetrically independent. This list was then incorporated into the input file used by CRUSH, which calculates vibration mode frequencies at each listed K point. We find that for each $\{\xi, \eta, 0\}$ wavevector thus calculated its lowest vibration mode frequency is always zero (allowing for a small float point error), i.e., RUMs exist for all $\{\xi, \eta, 0\}$ vectors in this structure.

Lattice vibrations of these rigid unit modes are found to involve all tetrahedra in the structure in complex translasive and rotational motions along all three directions, and they can't be decomposed to easily visualizable real space pictures.

Other well-known examples that possess both RUMs and NTE are β-quartz and cordierite used as a low thermal expansion material, and possibly many members from a growing number of framework silicates shown to have negative thermal expansion property, since occurrences of RUMs in these framework silicates are very frequent.

4.4.2. Structures with RUM but No NTE

CIT-5 (figure 4.2) has an orthorhombic structure with low symmetry of space group Im2a, with the point group of the space group being C_{2v} (mm2). The irreducible part of the Brillouin Zone is therefore only 1/8 of the whole Brillouin Zone. A 50×50×50 3-D grid occupying the parallelepiped defined by wavevectors *(0.5, 0, 0), (0, 0.5, 0)* and *(0, 0, 0.5)* was therefore used to generate a list of K points in search of possible RUMs, which we did find in this structure for all wavevectors on the plane (0, ξ, η). Its thermal expansion coefficient, however, is relatively large and positive, 14.9×10^{-6} /K (7) over the temperature range 373-973 K.

Quantitative thermal expansion studies have been performed only on a small and limited number of framework silicates, but decades of research over these structures as important practical materials give many indirect evidence that the majority of them do have positive thermal expansion coefficients, as expected from the common sense "fact" that materials expand when heated. On the other hand,

Rigid Unit Modes seem to be an almost universal occurrence to framework silicates. Therefore, a majority of AO_2 frameworks probably fall into this category.

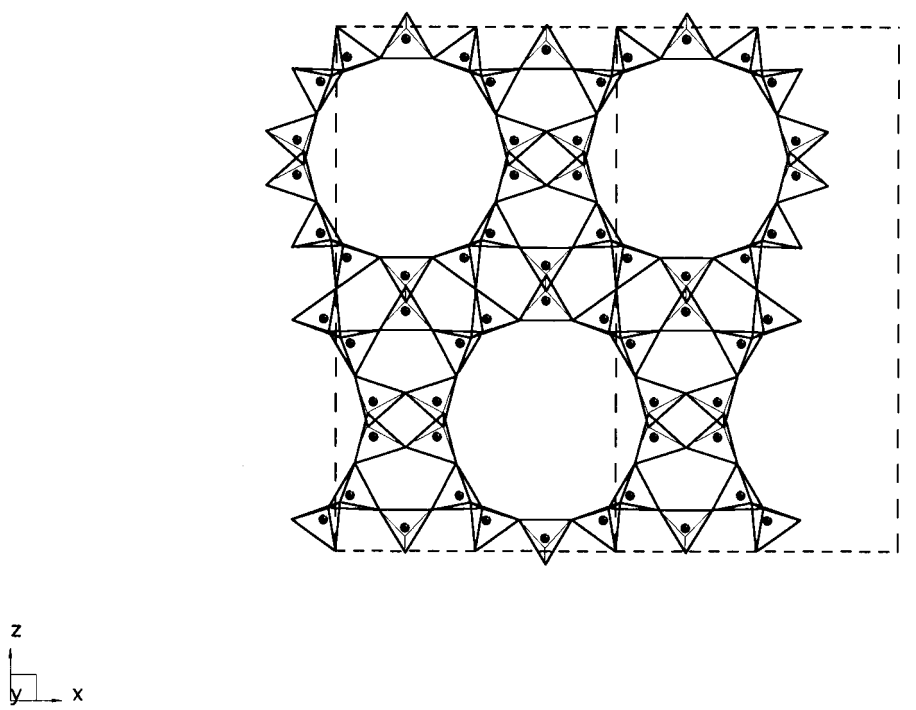

Figure 4.5. CIT-5 is a typical framework silicate with a 3-D network structure of corner sharing interconnecting Si-O tetrahedral.

4.4.3. Structures with No RUMs

Whether there are typical framework silicate structures that allow no RUMs is still an interesting open question. While it appears to be an exception for all other types of oxide frameworks discussed in the following sections, RUM seem to be almost universal here, and they are not restricted to higher symmetry structures either. From the hindsight, it is not surprising that all framework silicates calculated by CRUSH have RUMs in their structures, since SiO_4 tetrahedral building blocks in these networks are really rigid and ideal, together with the fact that except for quartz itself, almost all framework silicates are thermodynamically metastable and their structures are usually very "open", chances are very high that some thermal motions of the structure will leave SiO_4 tetrahedra intact, i.e., Rigid Unit Modes. Table 4.1 summarizes RUM studies in literature with respect to NTE.

Table 4.1 RUM vs. NTE in AO_2 network structures

Structure	Symmetry	RUM	Thermal Expansion Study	NTE
α-quartz	H	Y	Y	N
β-quartz	H, >848 °C	Y	Y	Y[8]
α-cristobalite	T	Y	Y	N
β-cristobalite	C, ~257 °C	Y	Y	Y[8]
Sodalite	C, ideal	Y	Y	N[9]
Sodalite	C	Y		
Sodalite	C	Y		
Cordierite	H	Y	Y (Thermal Material)	Y[10]
Cordierite	O, >1260 °C	Y		
Leucite	C, Ia3d, >687 °C	Y	Y	N[11]
Leucite	T, $I4_1/acd$	Y	Y	N[11]
Leucite	T, $I4_1/a$, <667 °C	N		
Tridymite	H	Y	Y	Y[12]
Kalsilite-Nepheline	H	Y	Y	N[13]
Feldspar	M	Y	Y	N[14]

4.5. $A_3M_2O_{12}$ network

Here constraint of common cation and anion valencies in solid state chemistry allows two possible combinations: +4 A cations with +6 M cations, or +6 A cations with +3 M cations. So far only compounds with the latter stoichiometry are found, where M cations could be Fe, Al, Y and +3 rare earth atoms, and A cations are W, Sc, Mo. Structures of these compounds are determined to be more or less identical 3-D corner sharing interconnecting AO_2 tetrahedra and MO_3 octahedra networks (Figure 4.6), with shapes of these polyhedra nonideal, and sizes varying with different A and M atoms. The best studied compounds of this family are $Sc_2(WO_4)_3$ (15) and $Y_2W_3O_{12}$ (16), both are of the same structure (space group *Pnca*, 60) with negative thermal expansion from very low temperature covering a wide range (-2.2×10^{-6}/k, 1-450 K and -7.0×10^{-6}/k, 15-1373 K respectively).

The point group of the space group *Pnca* is D_{2h} *(mmm)*, therefore a 50×50×50 3-D grid of K points (0~0.5, 0~0.5, 0~0.5) was used for CRUSH calculations to search out RUMs. Yet none of vibration modes of this list of wavevectors has zero frequency. Similar CRUSH calculations were performed for lower temperature lower symmetry monoclinic phase with symmetry of space group $P2_1/a$ (point group C_{2h}, *2/m*), and no zero frequency vibration modes were present either. Therefore we find no RUMs in this network structure type.

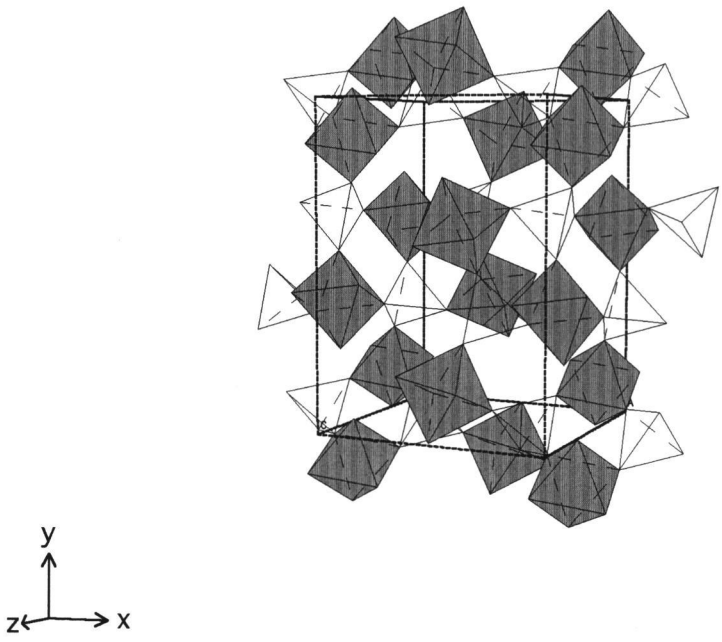

Figure 4.6. $Sc_2W_3O_{12}$ network consists of corner-sharing ScO_3 octahedra and WO_2 tetrahedra.

4.6. AMO_5 network

From the overall stoichiometry two possible combinations are possible: two +5 cations or one +4 cation plus one +6 cation. So far only compounds with former compositions are discovered, where A cations could be Nb, Ta, Mo, V, and M cations are P, V, As, P, S, Mo. They form a large family of compounds with corner-sharing interconnecting AO_2 tetrahedra and MO_3 octahedra as its basic structure unit and feature, which has been systematically studied by (17), with emphasis on their thermal expansion properties. Our RUM modeling shows that for one polymorph of this structure type, such as $NbOPO_4$, there are no RUMs in monoclinic $P2_1/c$ (point group C_{2h}, *2/m*) phases, one RUM at (½, 0, ½) in higher temperature orthorhombic *Pnma* (point group D_{2h}, *mmm*) phases. For the other polymorph, no RUMs exist in lower temperature tetragonal *P4/n* (point group C_{4h}, *4/m*) phase, compared to all {0, 0, ξ} wavevectors possessing RUMs in higher temperature higher symmetry *P4/nmm* (point group D_{4h}, *4/mmm*) phase. This is consistent with the fact that RUMs only appear when a structure is underconstrained, most often as the symmetry of a structure is high enough to reduce the independent number of constraints (or polyhedra links).

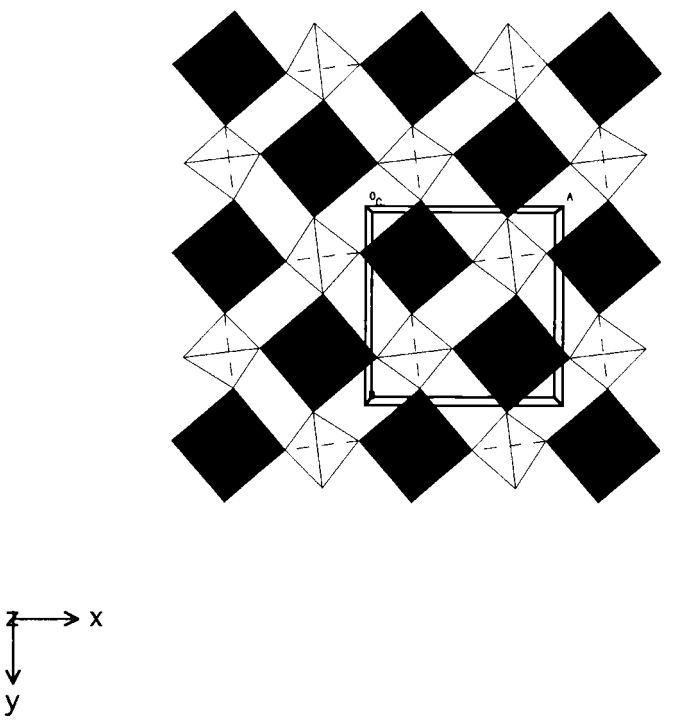

Figure 4.7. $NbOPO_4$ structure viewd down the tetragonal c axis.

4.7. MO_3 network

This type of network consists of purely corner-sharing cation-anion octahedral, which of itself can be ideal like in ReO_3 and (Nb)TaO_2F, (the structure then has the symmetry of space group *Pm-3m*), or distorted as in UO_3 and WO_3. (Nb)TaO_2F are found to have very small thermal expansion coefficients close to zero (chapter 2), and our CRUSH calculations show RUMs exist for all wavevectors {½, ½, ζ}, corresponding to "rocking motions" of octahedra along each of three axes.

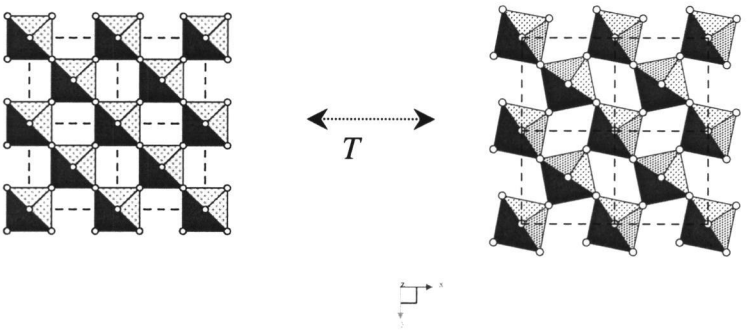

Figure 4.8. RUMs are reduced to polyhedra rocking motions in ideal corner-sharing octahedra MO_3 networks.

4.8. ZrW_2O_8 network

Outside framework silicates, ZrW_2O_8 appears to be the first material studied by RUM method (5), and for NTE materials it remains the most and best studied one (18-22). In terms of interconnecting polyhedra, one important structure feature separates this network out from all other four types discussed above: the system is exceptionally underconstrained in that all WO_4 tetrahedra have one corner that is unshared and linkage free, i.e., one out of four W-O bonds is non-bridging, while in other networks metal-oxygen bonds are all bridging ones and shared, all octahedral have 6 linkages and tetrahedral 4.

It is also striking that RUMs in ZrW_2O_8 don't contain any symmetry points in reciprocal space and those wavevectors with RUMs form a complex and irregular surface, unlike all other structures, where RUMs exist continuously on special symmetry branches and planes.

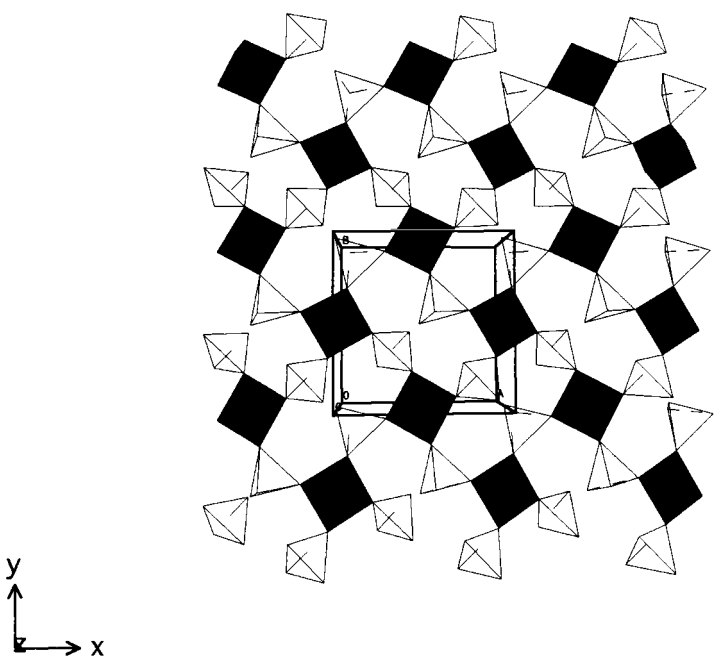

Figure 4.9. Structure of ZrW_2O_8 as a network of corner-sharing ZrO_3 octahedra and WO_2 tetrahedra.

4.9. Discussion

Table 4.2 summarizes results of RUM studies on all five types of octahedra-tetrahedra corner-sharing framework structures. Clearly a direct and simple correlation between existence of RUMs in a structure and negative thermal expansion property of the corresponding crystalline compound can not be established. It demonstrates that a framework oxide's possible negative thermal expansion property is not determined by its (idealized) network connectivity alone.

Table 4.2 RUM Model in NTE

STRUCTURE FAMILIES	NETWORK CONNECTIVITY	CRYSTAL SYMMETRY[A]	RUM[B]	NTE[C]
ReO_3 type (TaO_2F, NbO_2F)	Pure octahedral corner-sharing network	C	Yes	~ 0
$AOMO_4$ type (A=Nb, Mo…) (M=P, V…)	Octahedra:Tetrahedra=1:1	T, O, M	Yes and No	Yes and No
$A_2M_3O_{12}$ type (A=Al, Y, Lu…) (B=W, Mo)	Octahedra:Tetrahedra=2:3	O, M	No	Yes
ZrW_2O_8	Octahedra:Tetrahedra=1:2	C	Yes	Yes
ZrV_2O_7			No	
Framework silicates (quartz, zeolites, etc.)	Pure tetrahedral corner-sharing network	C, H, T, O	Yes	Yes

A) C-cubic, H-hexagonal, T-tetragonal, O-orthorhombic, M-monoclinic; B) and C) For the highest symmetry or typical structure types.

One possible problem could be that RUM method requires the tetrahedra and octahedra in a structure be rigid. In energy terms it implies those vibration modes that distort polyhedra, such as bending of O-A-O and O-M-O bond angels, should be very high in frequency/energy. For SiO_4 tetrahedra in Mg_2SiO_4, frequencies of these O-Si-O bond bending modes are between 13-20 THz (23), for WO_4 tetrahedra in $A_3M_2O_{12}$ type of network, one study (24) shows bending vibrations have frequency between 10-12 THz, consistent with measured values of 10-13 THz for internal vibration modes of WO_2 tetrahedra in the $CaWO_4$, the mineral scheelite (25). These values indicate that WO_2 tetrahedra are only about half as rigid as SiO_2 tetrahedra. More meaningful comparisons should probably be made within the same network structure between frequencies of polyhedra distorting modes, such as O-A-O or O-M-O bond bending ones, and those modes that preserve polyhedra more or less, which we attempt to model by RUMs. Unfortunately this either requires further development of RUM out of a purely geometrical modeling method, to take into account forces acting within a structure to be able to estimate any vibrational frequencies/energies, or some case-by-case adaptations of CRUSH program to bring in "force" factors in calculating each specific structure.

A related problem is that RUM model expects all polyhedra in a structure to be ideal, or idealized before computations are carried out. But because of symmetry (crystal class and space group) constraint of a structure, usually it doesn't allow its own building block polyhedra units to be idealized without destroying overall symmetry.

Lack of a direct and simple correlation between RUM and NTE of a structure being one thing, RUM modeling is still helpful in studying framework structures. In AO_2 type framework silicates it emphasizes the role of rigid and ideal SiO_2 tetrahedra as building blocks of these structures; with $A_3M_2O_{12}$ it draws attention to the fact that polyhedra in these structures are often less rigid and nonideal. In AMO_5 structure it appears to be behind the displacive phase transition that changes thermal expansion from positive to negative; with ZrW_2O_8 the strange distribution of RUMs in reciprocal space emphasizes once again how different this structure is from all other four types of networks.

4.10. References

1. K. D. Hammonds, M. T. Dove, A. P. Giddy, V. Heine, B. Winkler, *American Mineralogist*, 1057, 81 (1996)

2. A. P. Giddy, M.T. Pawley, G.S., and V. Heine, *Acta Cryst.* 697, A49 (1993)

3. K. D. Hammonds, M. T. Dove, A. P. Giddy, V. Heine, *American Mineralogist*, 1207, 79 (1994)

4. T.A. Mary, J.S.O. Evans, A.W. Sleight and T. Vogt, *Science,* 272, 90 (1996)

5. A. K. Pryde, K. D. Hammonds, M. T. Dove, V. Heine, J. D. Gale, M. C. Warren, *J. Phys.: Condens. Matter.* 10973, 8 (1996)

6. M.P. Attfield, A.W. Sleight, *Chem. Mater.*, 7, 10 (1998)

7. P. Lightfoot, D. A. Woodcock, M. J. Maple, L. A. Villaesusa and P. A. Wright, *J. Mater. Chem..*, 212, 11 (2001)

8. E. Bourova, P. Richet, *Geophys. Res. Lett.*, 2333, 25(1998)

9. D. Taylor, *Mineral. Mag.*, 761, 36(1968)

10. J. D. Lee, J. L. Pentecost, *J. Am. Ceram. Soc.*, 183, 59(1976)

11. D Taylor, C. M. B. Henderson, *Amer. Mineral*, 1476, 53(1968)

12. H. Schneider, O. W. Floerke, A. Majdic, Proc. Br. Ceram. Soc., 267, 28 (1979)

13. D. Taylor, C. M. B. Henderson, *Mineral. Mag.*, 708, 52(1988)

14. J. R. Mackert, S. W. Twiggs, A. L. Williams, *J. of Dent. Res.*, 1590, 79(2000)

15. J.S.O. Evans, T.A. Mary and A.W. Sleight, *J. Solid State Chem.*, 137, 148 (1998)

16. P.M. Forster and A.W.Sleight, Inter. *J. Inorg. Mater.*, 1, 123 (1999)

17. T. Amos, thesis submitted to the Oregon State University, 2001

18. A. P. Ramirez, G. R. Kowach, *Phys. Rev. Lett.* 4093, 80 (1998)

19. G. Ernst, C. Broholm, G. R. Kowach, A. P. Ramirez, *Nature* 396, 147 (1998)

20. W. I. F. David, J. S. O. Evans, A. W. Sleight, *Euro. phys. Lett.* 46, 661 (1999)

21. R. Mittal, S. L. Chaplot, *Solid State Communications* 319, 115 (2000)

22. T. R. Ravindran, A. K. Aroura, T. A. Mary, *Phys. Rev. Letters*, 17, 84 (2000)

23. G. D. Price, S. C. Parker and M Leslie, *Mineral. Mag.*, 157, 51 (1987)

24. J. Hanuza, M. Maczka, K. Hermanowicz, M. Andruszkiewicz, A. Pietraszko, W. Strek and P. Dereń, *J. of Solid State Chem.*, 49, 105 (1993)

25. V. C. Farmer, "The Infrared Spectra of Minerals", London: Mineralogical Society, 1974

Chapter 5

Free Energy Minimization of NTE Structures

5.1. Introduction

As shown in the previous chapter through RUM study of all types of framework oxides, where oxygen atoms are always two coordinated and bridge two metal-oxygen octahedra or tetrahedra (except for one out of four oxygen atoms in ZrW_2O_8), negative thermal expansion property of a structure can't be determined by its "geometry" part, i.e., network connectivity and crystal symmetries alone. To investigate further, the "force" part of a structure, namely interatomic interactions existing in a structure, needs to be taken into account. In this aspect increasingly more powerful and productive quantum mechanical methods have been developed and applied to solids, where all kinds of physical interactions between atomic and subatomic particles existing in a structure are represented by interacting quantum mechanical equations to various approximation levels, where the "force" part is automatically built-in, actually being the starting point and foundation of these methods. But the computation costs of these methods are really high, and often they emphasize physics of electrons in solids, none of them seem readily available or accessible to help study our specific problem of thermal expansion property of different types of framework oxides over a wide temperature range. Instead

essentially (semi)classical interatomic potential method appears a more accessible and valuable one to our purpose. In literature some potentials (1) have also proved to be as reliable for unit cell parameter predictions as quantum mechanic methods.

In this method a material is viewed as a periodic atomistic assembly, where two kinds of forces are in existence: one is the long range Columb force between cations and anions, the other the local two-body, three-body, or even four body interatomic potentials, with empirical or semi-empirical formulas and parameters. Structures and properties of this semi-classical mechanical system are then studied as a function of pressure and temperature.

Inclusion of pressure into this method is straightforward, since it only requires adding a PV term to the internal energy. Our study of thermal expansion property of framework oxides is restricted to ambient pressure so far, and compressibility of these materials are so high compared to it (10~100 GPa bulk modulus compared to 1×10^5 Pa for 1 atmosphere) that for practical purpose we can treat them as in vacuum, Helmholtz and Gibbs free energies being identical.

To introduce temperature into these types of simulations, three kinds of techniques are available: Molecular Dynamics (MD), Monte Carlo methods (MC) and free energy minimization (FEM). The last is a more recent development and application, also largely out of theoretical and computational studies of structure-property relationships in silicates (2-4), just like RUM method presented in previous chapter. In FEM Helmholtz free energy is first calculated, which includes the statical lattice energy summing over all Columb pairs plus two-body three-body

interatomic potentials, and the vibration free energy through vibration partition function. Structure parameters (lattice parameters and atom coordinate positions) are then adjusted until a minimal free energy configuration is obtained, and repeating this process at various temperatures enables direct calculations of thermal expansion of a structure. For our study of thermal expansion properties of bulk solids, FEM appears a direct and attractive route: first it takes into account vibration quantum effects such as zero point energies properly, therefore produces better results below the Debye temperature, and interpretation of normal vibrations generated by computations could reveal explicitly underlying mechanisms responsible for thermal expansions and phase transitions; second, it avoids statistical uncertainty associated with first two methods, which rely on computational costly numerical integration to minimize the problem, therefore also runs much faster.

The free energy minimization method has been successfully applied in studying thermal expansion behavior of several types of zeolites and $AlPO_4$, leading to interesting predictions of negative thermal expansion in advance of experiment investigations (5). It has also been preformed on ZrW_2O_8 (6), although exact implementation of the method is not clear and some of its results are not consistent with more recent experimental work (7, 8). This part of the thesis work is aimed at exploring the possibility of studying thermal expansion property of different types of framework oxides by a single uniform implementation of free energy minimization method, a general utility lattice program GULP (9).

5.2. Free Energy Minimization Method

There are three main concerns in successful application of FEM method, one lies in the theory underlying FEM itself, the second in the method being used, and the third in its practical application to structures we study.

5.2.1. Quasiharmonic Approximation

Application of the FEM method relies on validity of quasiharmonic approximation, which treats lattice vibrations as harmonic oscillators whose frequency vary with cell volume. Anharmonic effects, such as thermal expansion itself, only appear because temperature change induces cell volume change (as discussed in Chapter 1), and cell volume change in turn causes vibration frequency changes, which is the root cause for any anharmonic effects. In practice this limits the temperature range that can be studied by this method to about half of the melting point of the material (10). Still for ionic solids with high melting points we are studying this range seems adequate, and quasiharmonic approximation (QHA) itself appears to be the most accessible theoretical framework within with negative thermal expansion of oxide solids could be satisfactorily explained and understood (Chapter 1).

5.2.2. ZSISA Approximation

One reason that free energy minimization has been a late development among interatomic potential methods (compared to MD and MC) is the difficulty in efficient structure optimization, which requires evaluating derivatives of the free energy with respect to structural parameters. The theory, algorithms and computer programs that implement the method became available only recently, and in practice they often involve a more limiting approximation called zero static internal stress approximation (ZSISA), where instead of a full dynamic relaxation with respect to all structure parameters, including both "external coordinates" which determine lattice parameters and "internal coordinates" which describe individual atom positions inside a cell, the dependency of vibrational part of the free energy on "internal coordinates" is simply ignored. For a structure whose thermal expansion mainly changes lattice parameters but not internal variables associated with atoms in the cell, this approximation seems appropriate, but for structures whose "internal coordinates" vary significantly with temperature (compared to lattice parameter changes), ZSISA often fails at elevated temperature before QHA, lowering the upper limit in temperature where FEM is applicable.

5.2.3. Potential Models

Success of any interatomic potential methods largely depends on quality of potential models employed, which are usually derived in either of two possible ways. First is to determine the type of potentials and its parameters from higher level calculation, such as quantum mechanic ones, by attempting to reproduce an energy hypersurface. Secondly one can perform empirical fitting and try to reproduce experimental values of structure parameters and thermodynamic properties. Since potential parameters are second derivatives of energy with respect to structure parameters, good empirical fitting often requires quality experimental data of second derivative properties of solids, such as bulk modulus, elastic constants and dielectric constants, which usually are lacking for uncommon structures and difficult to determine experimentally.

Among five types of framework structures studied by RUM method, only two of them, AO_2 silicates and ZrW_2O_8, have potential models available in the literature to be used in FEM calculation, as discussed respectively in the following. All calculations have been performed using GULP kindly provided by the author of the program.

5.3. $AlPO_4$-17

$AlPO_4$-17 was found to experience a very strong negative thermal expansion over the temperature range 18-300 K, with a linear coefficient of thermal expansion of -11.7×10^{-6} /K (11). The structure is typical of framework silicates, a 3-D network of corner-sharing tetrahedra that are almost perfect and alternate between PO_2 and AlO_2. There are 108 atoms in each unit cell, but high symmetry of the structure (space group $P6_3/m$) reduces independent ones to 11.

5.3.1. Potential Model

The potential model used for $AlPO_4$-17 calculations is a two-body rigid ion model and doesn't include ionic polarizability and other local multi-body potentials explicitly, such as bond-bending force. It takes the basic form:

$$V(r) = \frac{q_i q_j}{r_{ij}} + Ae^{-\frac{r_{ij}}{\rho_{ij}}} - \frac{C_{ij}}{r_{ij}^6}$$

where q_i and q_j represent partial charges of the interaction, rij the interatomic distance between two ions, A, ρij and Cij are variable parameters that describe

short-range components of interatomic potentials, which is actually a Buckingham potential widely used in theoretical modeling of ionic solids.

This potential was recently developed using *ab initio* quantum mechanical methods, with parameters determined from the potential energy surface of a cluster and then fitted to the bulk property of a specific structure. It has been shown to be able to model silicates and aluminophosphates very accurately (5). The potential model and its parameters used in calculations are summarized in Table 5.1.

Table 5.1a Semiempirical potential parameters long range Columb component:

	Two-body long-range			
	O	Al	P	Unit
Z	-1.2	1.4	3.4	electrons

Table 5.1b Semiempirical potential parameters: short range Buckingham component:

	Two body short-range			
	O-O	Al-O	P-O	Unit
A	1388.7730	16008.5345	9034.2080	eV
ρ	0.3623	0.2085	0.1926	Å
C	175.0000	130.5659	19.8793	eV·Å^6

5.3.2. K space Sampling

The Helmholtz free energy of an ideal structure is the sum of its static internal energy, which would be calculated in conventional energy minimization using *V(r)*, and contributions from thermal vibrations:

$$A = U_{static} + (U_{vib} - TS_{vib})$$

The thermal vibration part is a sum over all the vibration modes throughout the Brillouin zone:

$$(U_{vib} - TS_{vib}) = \frac{1}{2}\sum_i \hbar\omega_i + kT\sum_i \ln(1 - e^{-\frac{\hbar\omega_i}{kT}})$$

GULP uses Monkhorse-Pack scheme to carry out this summation across the Brillouin zone for calculations of vibration modes (phonons), in which a grid is specified by the number of points along each axis, with the mesh being offset from the gamma point (origin of the Brillouin zone) to avoid symmetry problems. The required grid size is established by examining the convergence of FEM results, as summarized in Table 5.2:

Table 5.2. Convergence of $AlPO_4$-17 FEM runs with larger grid size in the Brillouin Zone

Grid size	# of K points	a (Å)	c (Å)	Free Energy (eV)
1	*1*	*13.352663*	*15.635637*	*-2105.201593*
2	*2*	*13.352520*	*15.635524*	*-2105.203866*
3	*10*	*13.352520*	*15.635503*	*-2105.203962*
4	*16*	*13.352526*	*15.635500*	*-2105.203979*
5	*39*	*13.352526*	*15.635500*	*-2105.203984*
6	*54*	*13.352528*	*15.635500*	*-2105.203987*

A grid size of 6×6×6 with 39 symmetry unique K points is found sufficient to converge all the observables to the required accuracy and therefore used for all following calculations.

5.3.3. *Free Energy Minimization of $AlPO_4$-17*

Free energy minimization was performed for $AlPO_4$-17 at 18 K, 75 K, 125 K and 190 K, with results plotted in figure 5.1:

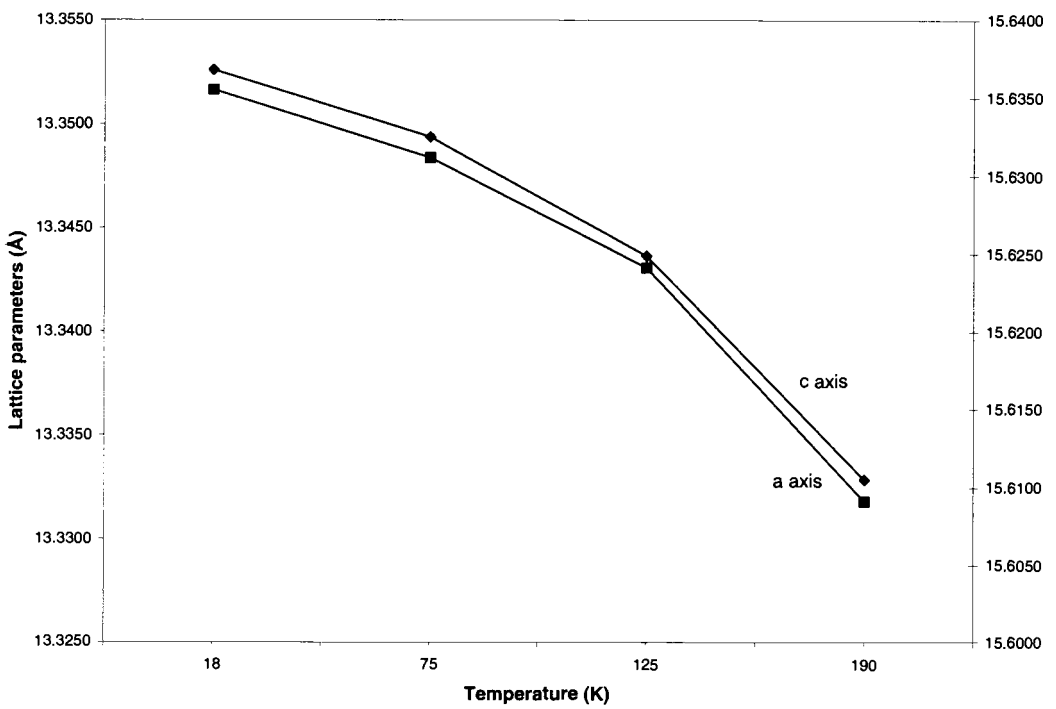

Figure 5.1. Calculated lattice parameter of $AlPO_4$-17 vs. temperature by FEM

Clearly, thus structure is found to experience negative thermal expansion, with a calculated volumetric thermal expansion coefficient about -2.25×10^{-5} /K.

Comparing it to the experimental value of -3.50×10^{-5} /K for $AlPO_4$-17 (11), it is clear that free energy minimization does successfully model the thermal expansion property of this structure on a semi-quantitative level.

However, the experimentally measured thermal expansion curve (lattice parameters vs. temperature) of $AlPO_4$-17 from 18 K to 300 K is close to linear, which implies the thermal expansion coefficient of $AlPO_4$-17 below room temperature is more or less a constant and temperature independent. This feature fits well with the Grüneisen model of thermal expansion as described in Chapter 1, yet is not reproduced by FEM calculations as illustrated in the figure above. This appears an unresolved issue in free energy minimization of framework zeolites, which is also present in other work (5).

The cause of this discrepancy is still not clear. While many approximations of both physical and numerical nature are involved in FEM modeling to generate errors, basic theory of thermal expansion does predict that close to 0 K thermal expansion coefficient will be proportional to T^3 (chapter 1) and temperature dependent; on the other hand whole profile fitting of powder XRD spectrum used to obtain experimental lattice parameter values also has its own share of systematic and numerical errors, which are often difficult to assess due to lack of other independent experimental means to measure thermal expansion with comparable precision and reliability.

Table 5.3 summarizes free energy minimization results of $AlPO_4$-17 at a fixed temperature. The difference between measured and calculated lattice parameters is

unusually large compared to other FEM calculations of silicate structures with similar potential models, which could be due to unresolved structure refinement issues of order-disorder between AlO_2 and PO_2 tetrahedra in experimental work of $AlPO_4$-17 (11).

Table 5.3 Free energy minimization results of $AlPO_4$-17 at 18 K

			Initial/expt.	Optimized/calc.
		a	13.8979 Å	13.3525 Å
		c	15.3302 Å	15.6355 Å
P	*12i*	*x*	0.9978	0.9978
		y	0.2383	0.2375
		z	0.1012	0.1013
P	*6h*	*x*	0.5730	0.5741
		y	0.9090	0.9083
		z	¼	
Al	*12i*	*x*	0.7633	0.7597
		y	0.9990	0.9988
		z	0.1009	0.0916

Table 5.3 (continued)

Al	*6h*	*x*	0.0940	0.0916
		y	0.4220	0.4246
		z	¼	
O	*12i*	*x*	0.0200	0.0243
		y	0.3450	0.3360
		z	0.1575	0.1607
O	*12i*	*x*	0.6490	0.6465
		y	0.9650	0.9658
		z	0.1685	0.1714
O	*12i*	*x*	0.0920	0.0942
		y	0.2009	0.2088
		z	0.1140	0.1115
O	*12i*	*x*	0.1330	0.1320
		y	0.2544	0.2489
		z	0.6261	0.6214
O	*12i*	*x*	0.2774	0.2716
		y	0.0030	0.0030
		z	1.0050	0.0083

Table 5.3 (continued)

O	*6h*	*x*	0.2370	0.2353
		y	0.4573	0.4517
		z	¼	
O	*6h*	*x*	0.4600	0.4644
		y	0.9159	0.9131
		z	¼	

The calculated phonon density of states for $AlPO_4$-17 at 18 K is plotted in Figure 5.2:

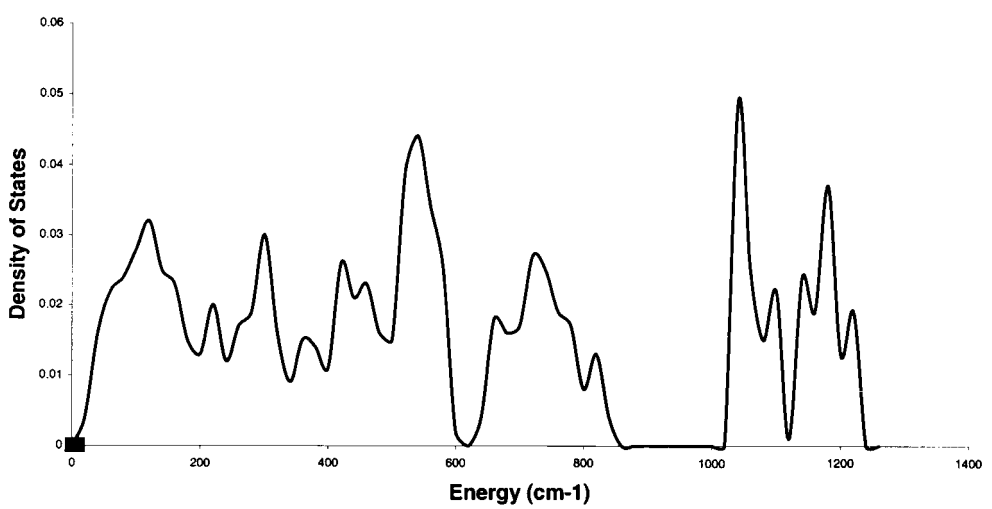

Figure 5.2. Calculated phonon density of states of $AlPO_4$-17 at 18 K.

At low energies (<60 cm^{-1}, or about 7.5 meV), the phonon spectrum shows the usual E^2 Debye feature, typical of crystalline materials but not as expected from the RUM model, which predicts a non-Debye like continuum of low energy vibration modes extending to almost zero energy for structures with many RUMs present. For ZrW_2O_8 accurate specific heat measurements and inelastic neutron scattering measurements have revealed the presence of an usual Debye like spectrum at low energies inconsistent with RUM modeling (12, 13); for $AlPO_4$-17 experimental data is lacking, but calculations here also predict an usual Debye spectrum at low energies, notwithstanding RUMs existing on all wavevectors $\{\xi, \eta, 0\}$ in this structure (Chapter 4).

5.3.4. Vibration Modes Responsible for NTE

One important advantage of the FEM method is its ability to calculate full phonon spectrum of a structure, which can then be used to find out which vibration modes are most responsible for negative thermal expansion of a NTE structure within the formalism of Grüneisen model as presented in Chapter 1.

With 108 atoms inside one unit cell, $AlPO_4$-17 structure has 3×108=324 branches in its phonon spectrum, their relative contributions to NTE of the structure are plotted in Figure 5.3:

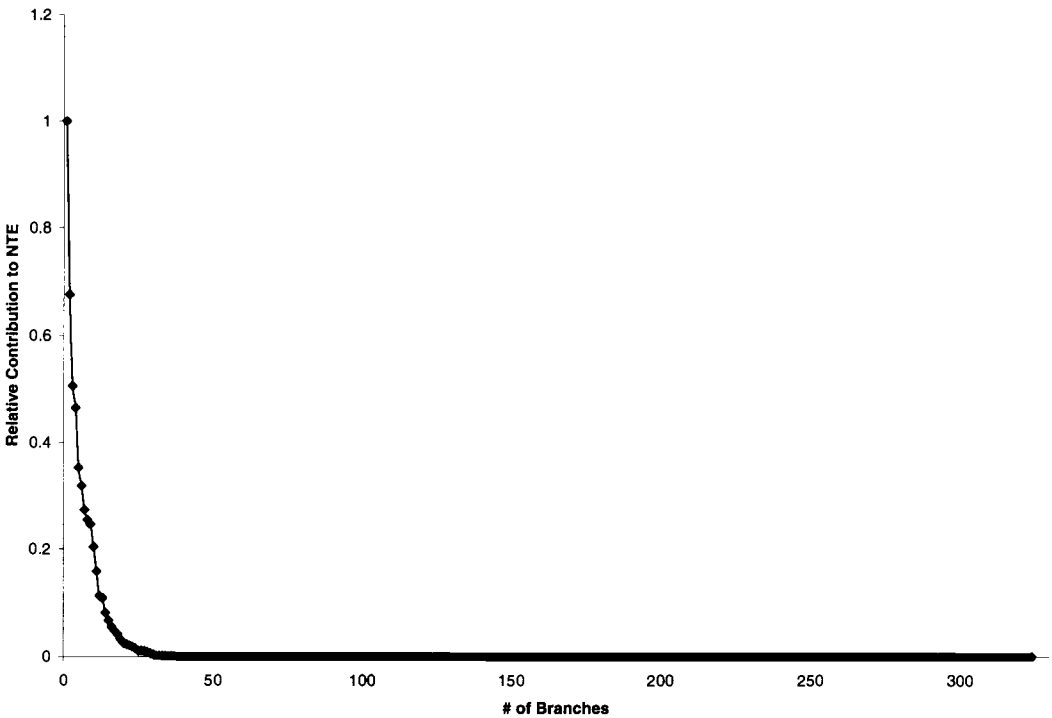

Figure 5.3. Each phonon branch's relative contribution to NTE in $AlPO_4$-17

Nothing is surprising here with low number branches contribute more to NTE with their lower vibration energies on average.

We can also integrate the phonon spectrum in another way to see vibration modes in which energy range are most responsible to NTE of the structure. Figure 5.4 shows that almost all the contribution to negative thermal expansion in $AlPO_4$-17 comes from vibration modes with energies below 15 meV.

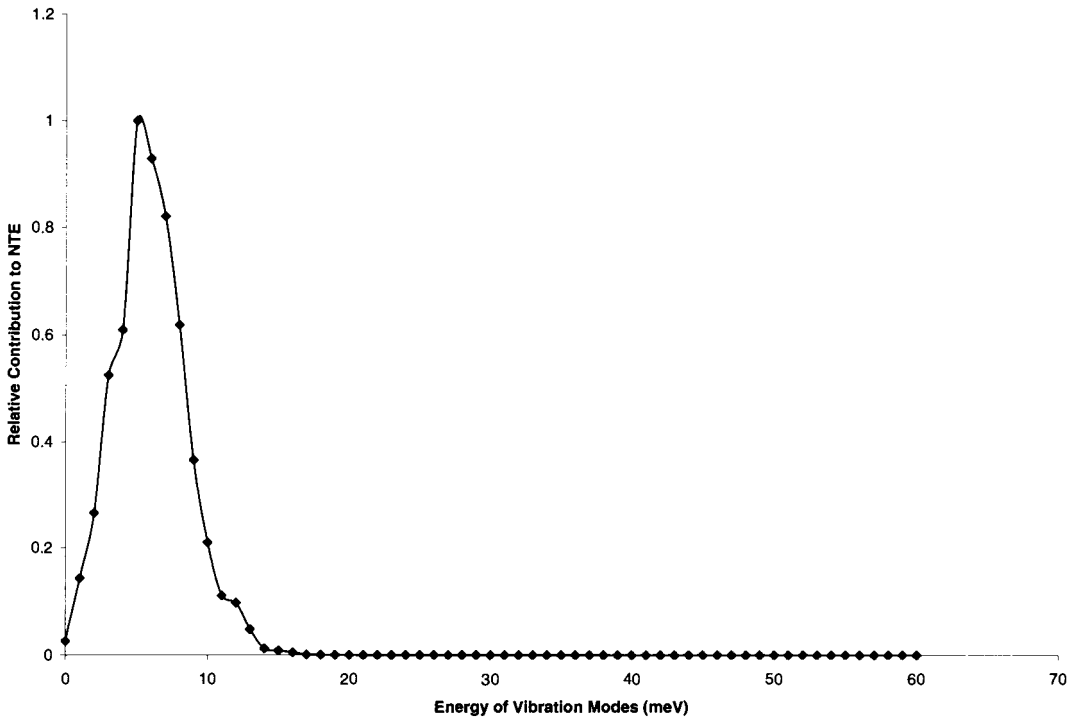

Figure 5.4. Relative contribution to NTE vs. vibration mode energy in $AlPO_4$-17

Figure 5.5 further shows how cross-sections of the Brillouin Zone contribute to NTE of this structure. One of them, $\{\xi, \eta, 0\}$, is where all RUMs in this structure are located (Chapter 4), but neither is it where the maximum relative contribution to NTE is located, nor does it have a discernable larger contribution than other planes in the Brillouin Zone. This contradicts what one would expect from an oversimplified interpretation of RUM modeling results, which predicts that RUM modes are most responsible for NTE in $AlPO_4$-17.

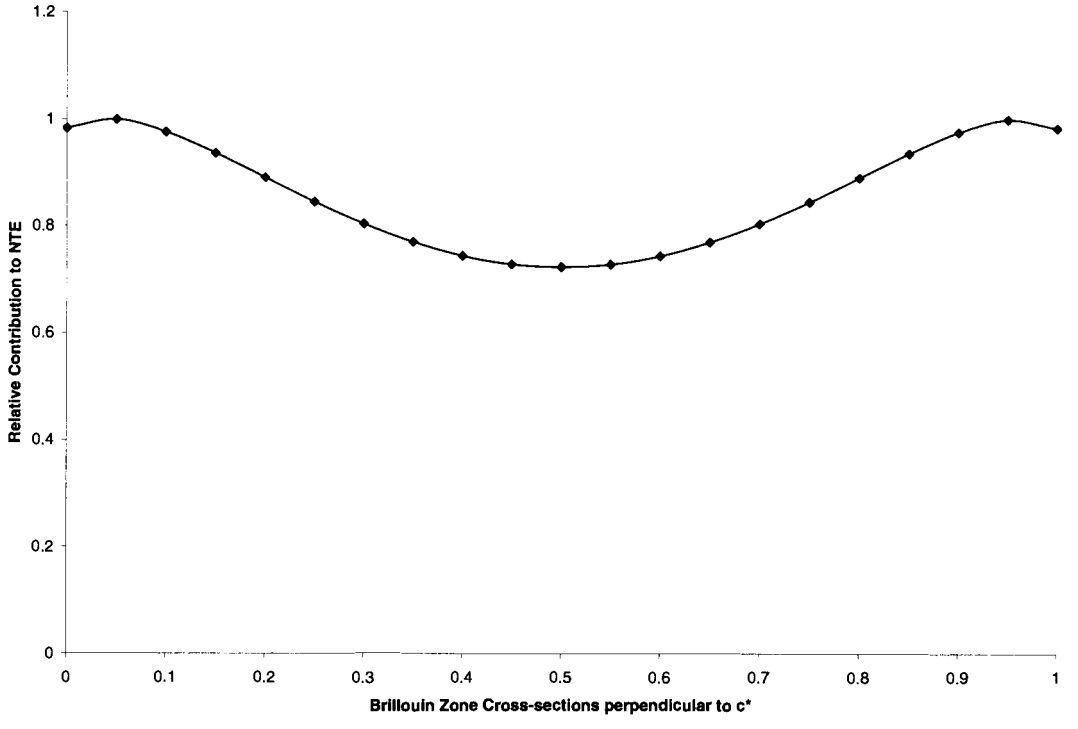

Figure 5.5. Relative contribution to NTE from each cross-sections in the Brillouin zone perpendicular to c^*

5.4. ZrW_2O_8

Cubic α-ZrW_2O_8 is observed to show large isotropic thermal expansion over a wide temperature range. The structure consists of interconnecting corner-sharing ZrO_3 octahedra and WO_2 tetrahedra, with one corner out of four for each

tetrahedral being unshared and linkage free. There are 44 atoms in the unit cell, however symmetry of the structure (space group $P\ 2_13$) reduces independent ones to 7, four of them oxygen atoms.

5.4.1. Potential Model

The potential model adopted to calculate ZrW_2O_8 differs from the one for $AlPO_4$-17 in two aspects: first, polarizability of oxygen atoms is introduced by shell model, which has been widely used in modeling oxide solids, and increases independent particles inside the unit cell to 11, each oxygen atom represented by a positively charged core and a massless negatively charged shell, with a spring connecting each pair; second, a special covalent potential is introduced between the nearest W and O atoms, which appears to represent some many-body forces implicitly. It turns out both additions are essential to FEM calculations of ZrW_2O_8, especially the special covalent potential, neglecting it would lead to a positive thermal expansion, which is not physically correct. These interatomic potentials have following forms:

$$V(r) = \frac{q_i q_j}{r_{ij}} + Ae^{-\frac{r_{ij}}{\rho_{ij}}} - \frac{C_{ij}}{r_{ij}^6}$$

The general potential in the structure, which is the usual Columb long range potential plus a Buckingham short range potential;

$$V_{core-shell} = \frac{1}{2}\kappa r^2_{core-shell}$$

The shell model potential representing polarization of oxygen atoms in the structure, κ being the spring constant;

$$V_{w-o} = -De^{-\frac{n(r-r_0)^2}{2r}}$$

The special covalent potential between bonding W and O atoms, r_o has a fixed value of 1.79 Å, r being the distance between W and O atoms, D and n potential parameters.

Table 5.4 summarizes the potential model and parameters used for free energy minimization of ZrW_2O_8:

Table 5.4 Potential model and parameters of ZrW_2O_8

Atom 1	Atom 2	Potential	*A (eV)*	*ρ (Å)*	*C* *(eV·Å^6)*
O_{core}	O_{shell}	Spring (c-s)		*K=70 eV/Å^2*	
Zr	Zr	Buckingham	1822	0.1828	0
Zr	W	Buckingham	1822	0.1893	0
Zr	O_{shell}	Buckingham	1822	0.2568	0
W	W	Buckingham	1822	0.1957	0
W	O_{shell}	Buckingham	1822	0.2633	0
O_{shell}	O_{shell}	Buckingham	1822	0.3308	100
W	O_{shell}	Covalence	D=5.0 eV, n=29.4 *Å^{-1}*, *r0=1.79 Å*		

5.4.2. Preparatory Conventional Energy Minimization

When running free energy minimization on a structure it is always best to optimize the system in a conventional calculation that minimizes static internal energy first, and then use the optimized structure as starting model for later free energy minimizations. The strategy offers two main advantages: first, ordinary internal energy optimization is much faster than free energy minimization, and given that thermal vibrations are only a small perturbation of a structure, this two-step approach could reach free energy minimum in the shortest amount of CPU time; second, the initial nonoptimized structure may have imaginary vibration modes present, particularly for shell models where oxygen shells are arbitrarily placed on top of cores at the start, which means the breakdown of calculations since imaginary modes means an unstable structure.

Table 5.5 summarizes the results of ordinary energy minimization of ZrW_2O_8 with the potential model discussed above:

Table 5.5. Conventional energy optimization of ZrW_2O_8. Except O1 and O2, other atoms all have 3-fold symmetry.

		Initial/expt.	Optimized/calc.
	a	9.1600 Å	9.1697 Å
Zr	x	0.0003	0.0020
W1	x	0.3412	0.3676
W2	x	0.6008	0.5952
O1	x	0.2071	0.2089
	y	0.4378	0.4514
	z	0.4470	0.4547
O2	x	0.7876	0.7846
	y	0.5694	0.5614
	z	0.5565	0.5491
O3	x	0.4916	0.4821
O4	x	0.2336	0.2510

5.4.3. K space Sampling Size

Just as in the case of $AlPO_4$-17, free energy minimization was performed as a function of the grid size in Brillouin zone to find the optimal size for later computations:

Table 5.6 Convergence of ZrW_2O_8 FEM runs with larger grid sizes in the Brillouin Zone

Grid Size	Number of K points	a *(Å)*	Free energy *(eV)*
6×6×6	11	9.171631	-885.211905
9×9×9	46	9.171634	-885.211946
12×12×12	76	9.171634	-885.211916
20×20×20	340	9.171633	-885.211918

A grid of 20×20×20 including 340 symmetry unique K points was found to be sufficient and used for all the following calculations.

5.4.4. Free Energy Minimization of ZrW_2O_8

Full minimization of the free energy with respect to both strains (lattice parameters) and fractional coordinates was found to be highly unstable for ZrW_2O_8 using GULP and the potential model described above. Above 30 K it fails due to the appearance of soft modes (with zero frequency) in the Brillouin zone, reducing the number of vibration modes from 44×3=132 to 130 or 131. Ultimately these modes become imaginary and the structure unstable. In contrast, free energy minimization performed under the ZSISA approximation doesn't suffer the same difficulty until above 500 K, when soft modes appear again and the method breaks down. This is different from FEM modeling of silicate structures such as quartz (12), where full FEM breaks down similarly at room temperature due to appearance of soft modes, but ZSISA works all the way up to 1000 K. The difference seems to suggest the failure has more to do with inadequacy of the potential model adopted for ZrW_2O_8 than the FEM method itself.

As a consequence of the above, only free energy minimization in the zero static internal stress approximation is considered for ZrW_2O_8, with results plotted in Figure 5.2. The calculated thermal expansion coefficient is about -5.53×10^{-6} /K compared to the experimental value of -8.7×10^{-6} /K.

Above 400 K or so the thermal expansion curve shows larger and larger deviation from the general trend of a straight line, until it reaches 500 K and then free energy minimization under ZSISA fails too due to reappearance of soft modes.

The failure is probably due to a combination of inadequacy of the potential model being used and deficiencies of the FEM method as implemented by GULP.

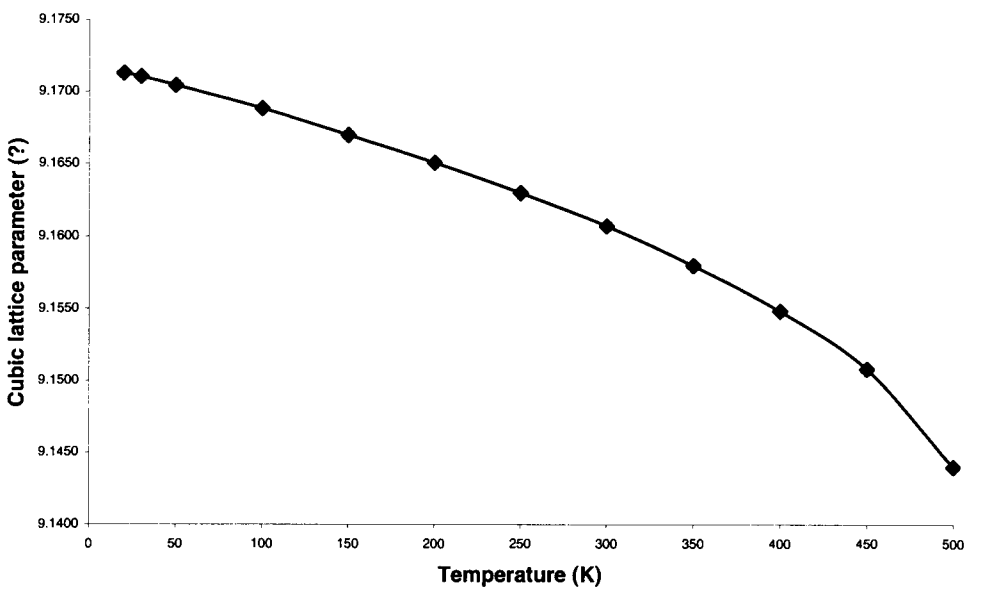

Figure 5.6. Calculated lattice parameter of ZrW_2O_8 vs. temperature by FEM

Table 5.7 summarizes free energy minimization results of ZrW_2O_8 at a fixed temperature. The calculated structure parameters are in good agreement with experimentally determined ones.

Table 5.7. Free energy minimization results of ZrW_2O_8 at 20 K

		Initial/expt.	Optimized/calc.
	a	9.1697 *Å*	9.1713 *Å*
Zr	*x*	0.001975	0.001969
W1	*x*	0.367586	0.367603
W2	*x*	0.595210	0.595194
O1	*x*	0.208884	0.208909
	y	0.451377	0.451379
	z	0.454661	0.454646
O2	*x*	0.784607	0.784564
	y	0.561403	0.561381
	z	0.549062	0.549055
O3	*x*	0.482082	0.482082
O4	*x*	0.251040	0.251077

The calculated phonon density of states for ZrW_2O_8 at 20 K is plotted in Figure 5.7:

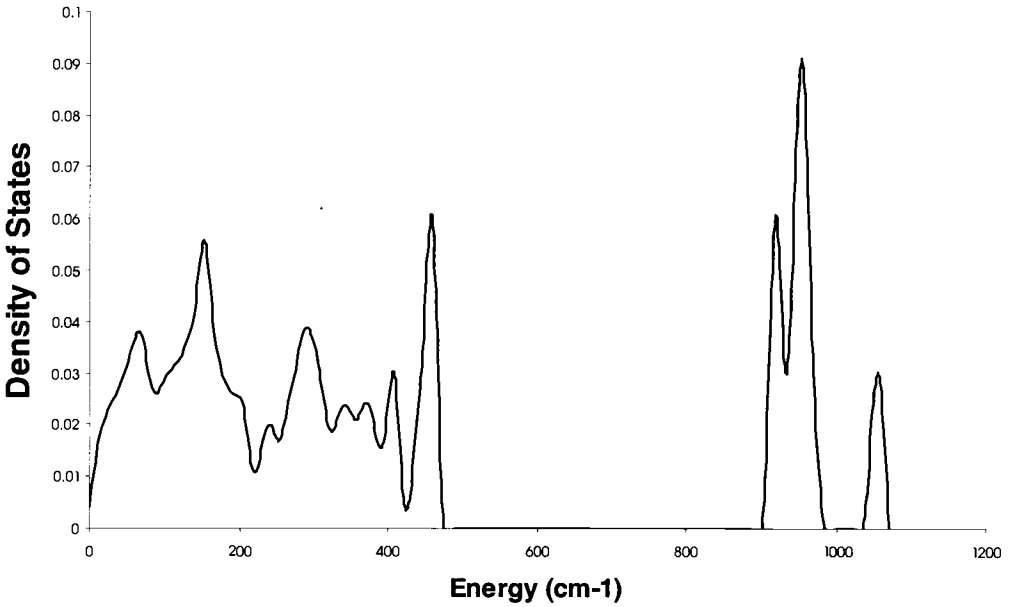

Figure 5.7. Phonon density of states of ZrW_2O_8 at 20 K

The low energy phonon spectrum is still Debye type with E^2 energy dependency, which agrees with inelastic neutron scattering measurements (11) but contradicts what one might expect from RUM modeling of this structure.

With 44 atoms inside one unit cell, the phonon spectrum of ZrW_2O_8 has 44×3=132 branches. The relative contribution to NTE of each branch is plotted in Figure 5.8:

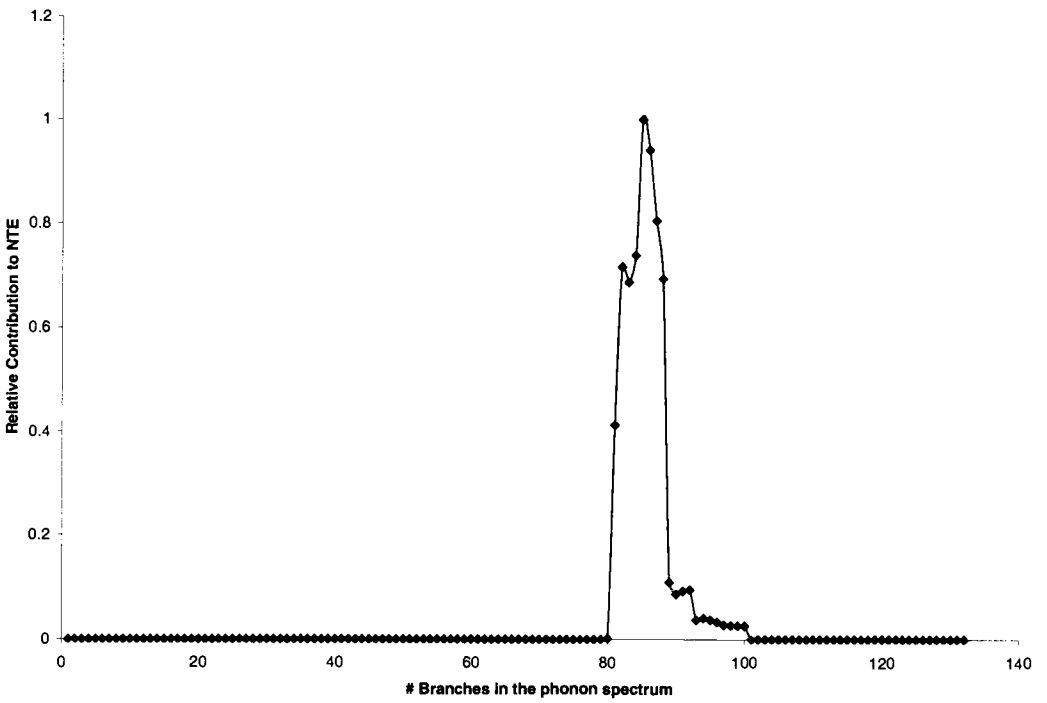

Figure 5.8. Each phonon branch's relative contribution to NTE in ZrW_2O_8

The relative contribution to NTE vs. vibration mode energy in ZrW_2O_8 is plotted in Figure 5.9:

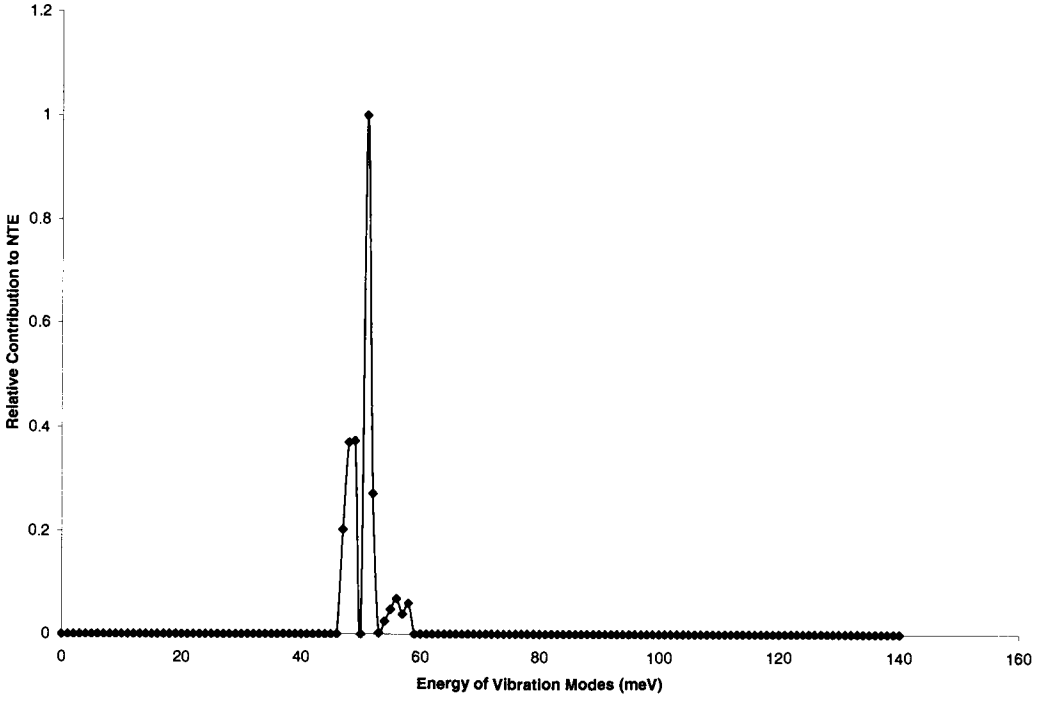

Figure 5.9. Relative contribution to NTE vs. vibration mode energy in ZrW_2O_8

These results are a little puzzling: vibration modes with energies between 40~60 meV appear to be most responsible for NTE in ZrW_2O_8, yet at low temperature these modes could hardly be excited, as thermal energy at 30 K is about 2.5 meV, where the structure does experience negative thermal expansion. Again inadequacy of the potential model we adopted is probably the main reason results obtained concerning ZrW_2O_8's phonon spectrum are not physically reasonable, even though they do predict negative thermal expansion for the structure correctly.

5.5. Discussion

Compared to other computation methods, FEM has its strength in relatively low computation cost and the ability to predict structure and thermodynamic properties of bulk inorganic solids reliably. Applying it to model thermal expansion property of framework oxides is successful, yet not without its problems that need more future work, among which lack of consistent and reliable potential models for oxide structures with transition metals present appears most troubling.

Direct comparison of lattice parameters of a structure calculated by FEM with experimentally determined ones must be made with care, since there are important systematic errors in lattice parameter values from both sides, and there are few independent means to verify reliability of each.

5.6. References

1. J. D. Gale, *J. Phys. Chem B*, 5423, 102 (1998)

2. L. N. Kantorovich, *Phys. Rev. B* 3520, 51 (1995)

3. L. N. Kantorovich, *Phys. Rev. B* 3535, 51 (1995)

4. M. B. Taylor, G. D. Barrera, N. L. Allan, T. H. K.. Barron, *Phys. Rev. B* 14380, 56 (1997)

5. P. Tschaufeser, S. C. Parker, *J. Phys. Chem.* 10609, 99 (1995)

6. R. Mittal and S. L. Chaplot, *Phys. Rev. B* 60 (1999)

7. T. R. Ravindran, A. K. Aroura, T. A. Mary, *Phys. Rev. Letters*, 17, 84 (2000)

8. D. Cao, F. Bridges, G. R. Kowach, A. P. Ramirez, publication preprint(2001)

9. J. D. Gale, *J. Chem. Soc., Faraday Trans.*, 629, 93 (1997)

10. D. J. Lacks, G. C. Rutledge, *J. Chem. Phys.*, 9961, 101, 1994

11. M. P. Attfield, A.W. Sleight, *Chem. Mater.*, 7, 10 (1998)

12. A. P. Ramirez and G. R. Kowach, *Phys. Rev. Lett.* 4903, 80 (1998)

13. G. Ernst, C. Broholm, G. R. Kowach, and A. P. Ramirez, *Nature* (London) 396, 147 (1998)

Chapter 6

Conclusions and Further Discussions

6.1. Material-Structure-NTE

The two questions asked in Chapter 1 as introduction to this thesis work, "what (other) structures/materials show NTE?", and "why these structures/materials show NTE but not others?", have been partially answered now, or further clarified to more workable forms.

For inorganic solids at high temperature, so far only structures with two-coordinated oxygen are found to possess negative thermal expansion property. Two coordination, or in terms of chemical bonding linear (or close to it) M-O-M bonds, is not oxygen's most common coordination number in solids, as witnessed by limited type of structures that support this chemical environment: only 5 of them. It appears NTE rises largely out of openness of a structure created by these two-coordinated structures, which is usually rationalized in terms of certain special vibration modes capable of decreasing its energy with contracted lattices, and formalized by the Grüneisen Model.

On a structure by structure basis, thermal expansion property of an inorganic solid could be accurately and reliably determined, as the example of TaO_2F and NbO_2F in chapter 2 showed; their structural features could be easily modeled,

which RUM method in chapter 4 typifies, even structure itself and thermal expansion coefficient could be successfully computed and predicted, with semi-quantitative quality, as shown in chapter 5. Yet an overall clear picture of material-structure-NTE relationship is still out of reach.

We can certainly endeavor to reach such a goal, or try to get as close to it as possible. There appear to be several clues or directions along which future work on thermal expansion property of crystalline materials, which NTE researches spearhead, could be conducted. One is the mysterious relationship between (displacive) phase transitions and (negative) thermal expansion; the other concerns those elusive special vibration modes with negative Grüneisen parameters, which currently are thought of as real reasons responsible for NTE.

6.1.1. Displacive Phase Transition in NTE Structures

As aforementioned in chapter 1, there appears to exist certain interesting correlation between displacive phase transitions and negative thermal expansion property. A good example is monoclinic to orthorhombic phase transition in $Sc_2W_3O_{12}$ structure of $A_3M_2O_{12}$ type network, which can be viewed as a 3-D network of corner-sharing ScO_3 octahedra and WO_2 tetrahedra. At around 180 K the structure transforms from a lower symmetry monoclinic $P\ 2_1/a$ phase to a higher symmetry orthorhombic $P\ n\ c\ a$ phase and cell volume is halved. In Figure

6.1 the lattice parameters of orthorhombic phase as a function of temperature is plotted (ref):

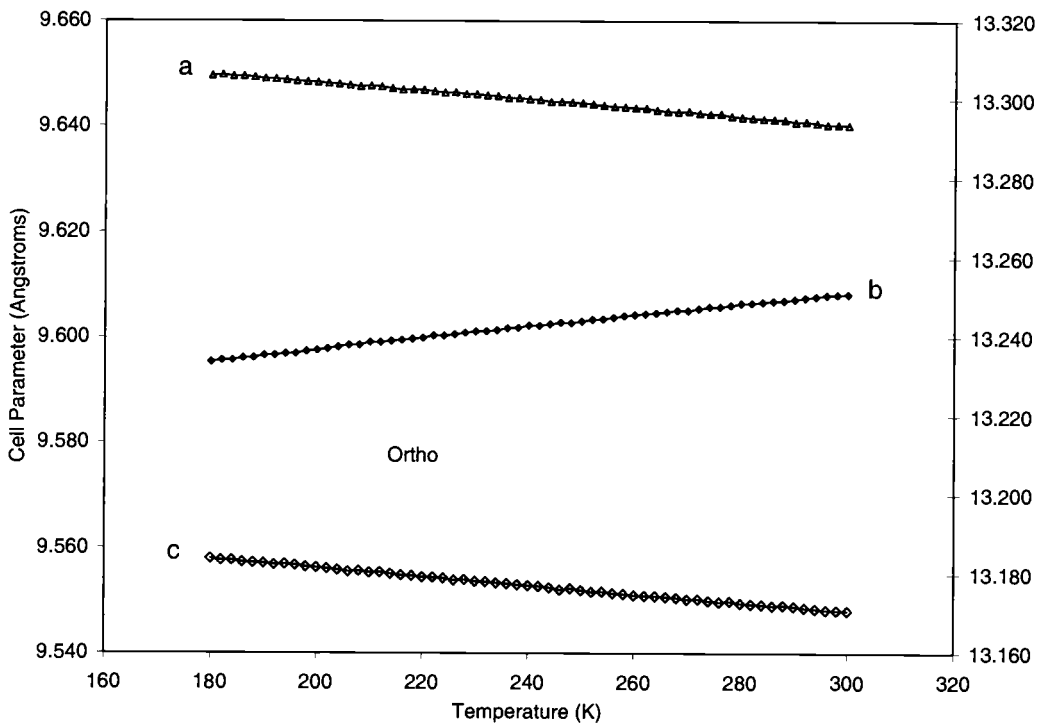

Figure 6.1. Lattice parameters of $Sc_2W_3O_{12}$ orthorhombic phase vs. temperature

And two lattice parameters of the monoclinic phase as a function of temperature were plotted in Figure 6.2:

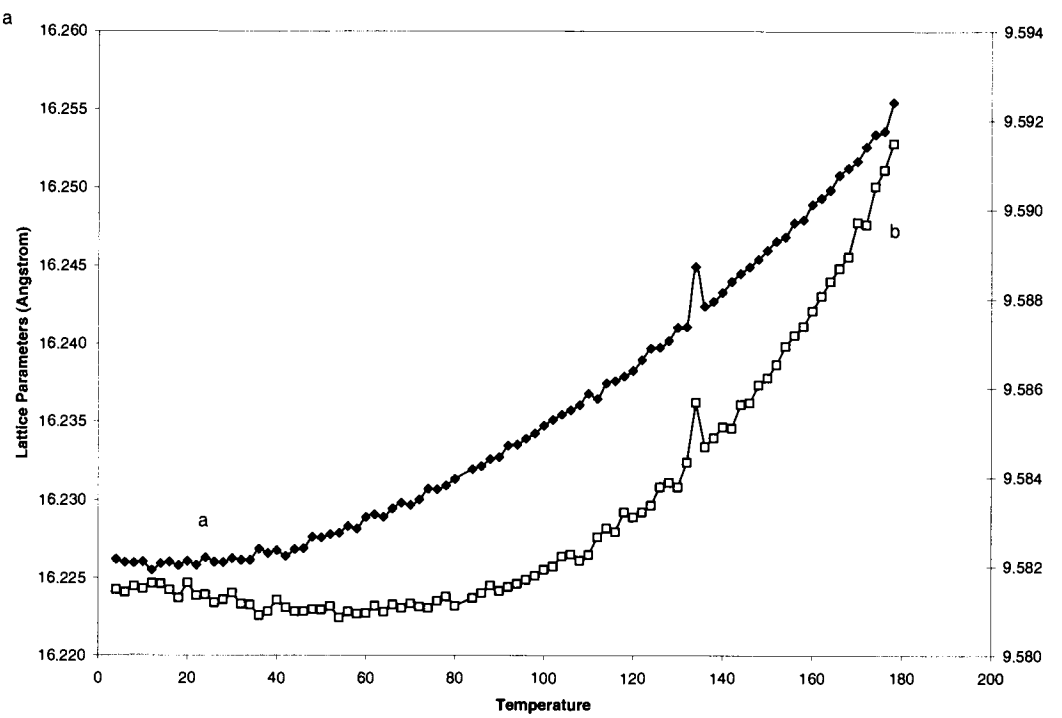

Figure 6.2. Lattice parameters of $Sc_2W_3O_{12}$ monoclinic phase vs. temperature

Comparing the orthorhombic unit cell with half of that monoclinic cell (the other half could be generated by 2_1 symmetry operation), the transformation matrix is:

$$\begin{pmatrix} \bar{a}_{mono} \\ \bar{b}_{mono} \\ \bar{c}'_{mono} \end{pmatrix} = \begin{pmatrix} 0 & -1 & 1 \\ -1 & 0 & 0 \\ 0 & 0 & -1 \end{pmatrix} \begin{pmatrix} \bar{a}_{ortho} \\ \bar{b}_{ortho} \\ \bar{c}'_{ortho} \end{pmatrix}$$

Or from monoclinic to orthorhombic phases:

$$\begin{pmatrix} \bar{a}_{ortho} \\ \bar{b}_{ortho} \\ \bar{c}'_{ortho} \end{pmatrix} = \begin{pmatrix} 0 & -1 & 0 \\ -1 & 0 & -1 \\ 0 & 0 & -1 \end{pmatrix} \begin{pmatrix} \bar{a}_{mono} \\ \bar{b}_{mono} \\ \bar{c}'_{mono} \end{pmatrix}$$

with $\bar{c}'_{ortho} = \frac{1}{2}\bar{c}_{ortho}$.

With the help of this transformation matrix we can compare lattice parameter changes of two phases directly using the orthorhombic unit cell as one uniform reference, as illustrated in Figure 6.3:

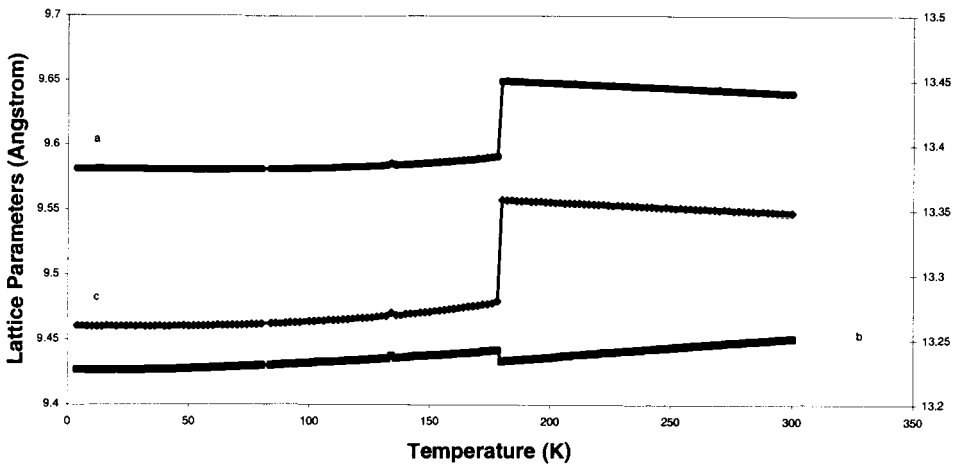

Figure 6.3a. Lattice parameter a, b and c change with temperature in mono-ortho phase transition

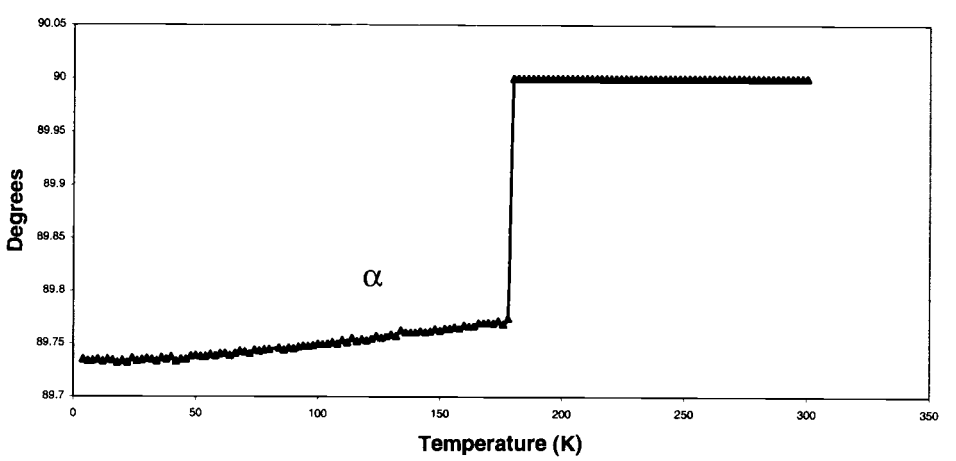

Figure 6.3b. Lattice parameter α change with temperature in mono-ortho phase transition

Clearly for this phase transition NTE only immediately appears after the phase transition point in higher temperature higher symmetry form. This feature is also present in AO_2 network, where α-quartz has a displacive phase transition around 846.15 K transforming to β-quartz, which experiences negative thermal expansion; in the A_2MO_7 network ZrV_2O_7, ZrP_2O_7 shows this behavior; in the AMO_5 network $NbOPO_4$ and $TaOPO_4$. The correlation is not found in MO_3 network however, which also happens to be the one without an (obvious) NTE structure.

$NbOPO_4$ is an especially interesting example, as dynamic RUM motions on wavevectors $\{0, 0, \xi\}$ in higher temperature *P4/nmm* phase would destroy mirror plane symmetry operations of the structure, which is exactly what a second order phase transition in this structure does statically, reducing the overall symmetry to *P4/n,* and changing the thermal expansion coefficient from negative to positive. This example shows that phase transitions, RUMs and NTE are all intrinsically linked together, which is not surprising in itself since they are all lattice dynamic behaviors and determined by interatomic interactions within a crystallographic structure. We may hope further researches along this direction could help us understand structure-property relationship in NTE structures better, and any insights gained this way could be of some aid in discovering more materials with special thermal expansion properties.

6.1.2. Vibration Modes Responsible for NTE

So far NTE is only interpreted or studied within the theoretical framework of quasiharmonic approximation, the larger question of whether this model's range of validity covers NTE is more or less untouched. Even assuming quasiharmonic approximation is adequate to the task, for the best studied structure ZrW_2O_8 itself, no consensus has been reached on what vibration modes are responsible for NTE. There is also considerable discrepancy between lattice dynamic calculations, RUM modeling and more detailed experimental studies which need to be further worked on.

6.2. More work ahead

Too many questions, too few answers. And real solutions to any problems become new problems themselves. The best we can hope is to get better and better at finding new solutions or more answers. Negative thermal expansion is no exception, and hopefully this thesis adds a little to its further understanding as well as utilization, no matter how small it is.

Bibliography

T. G. Amos, *Thesis* submitted to the Oregon State University, (2000)

S. Andersson, *Acta Chem. Scand.*, 2233, 18 (1964)

N. W. Ashcroft and N. D. Mermin, "Solid State Physics", p. 492, Saunders College, 1976

M. P. Attfield, A.W. Sleight, *Chem. Mater.*, 7, 10 (1998)

M. Blackman, *Philos. Mag.* 9, 831 (1958)

E. Bourova and P. Richet, *Geophysical Research Letters,* 13, 25, 2333 (1998)

W. R. Buessem, "Mechanical Propertiese of Engineering Ceramics", (W. W. Kreigel and H. Palmour III, Eds.), P. 127. Interscience, NY 1961

D. Cao, F. Bridges, G. R. Kowach, A. P. Ramirez, publication preprint

W. I. F. David, J. S. O. Evans, A. W. Sleight, *Euro. phys. Lett.* 46, 661 (1999)

M. T. Dove, "Introduction to Lattice Dynamics", p.173, p.61, Cambridge University Press, 1993

Niangao Duan, A. W. Sleight etc, *J. Solid State Chem.*, 424, 139(1998)

Niangao Duan, A. W. Sleight etc, *J. Amer. Chem. Soc.*, 8694, 122(2000)

G. Ernst, C. Broholm, G. R. Kowach, and A. P. Ramirez, Nature (London) 396, 147 (1998)

J.S.O. Evans, T.A. Mary and A.W. Sleight, *J. Solid State Chem.*, 137, 148 (1998)

V. C. Farmer, "The Infrared Spectra of Minerals", London: Mineralogical Society, 1974

P. M. Forster, A. Yokochi and A.W.Sleight, *J. Solid State Chem.*, 140(1), 157 (1998)

P. M. Forster and A.W.Sleight, Inter. *J. Inorg. Mater.*, 1, 123 (1999)

L. K. Frevel and H. W. Rinn, *Acta Cryst.*, 626, 9 (1956)

A. P. Giddy, M. T. Dove, G. S. Pawley and V. Heine, *Acta, Cryst.* 697, A49(1993)
K. D. Hammonds, M. T. Dove, A. P. Giddy, V. Heine, *American Mineralogist*, 1207, 79 (1994)

K. D. Hammonds, M. T. Dove, A. P. Giddy, V. Heine, B. Winkler, *American Mineralogist*, 1057, 81 (1996)

J. Hanuza, M. Maczka, K. Hermanowicz, M. Andruszkiewicz, A. Pietraszko, W. Strek and P. Dereń, *J. of Solid State Chem.*, 49, 105 (1993)

N. Khosrovani, A. W. Sleight, *J. Solid State Chem*, 2, 121 (1996)

V. Korthius, N. Khosrovani, A. W. Sleight, N. Roberts, R. Dupree and W. W. Wareen Jr., *Chem.. Mater.*, 7, 412 (1995)

A. C. Larson and R. B. Von Dreele, LANSCE, Los Alamos National Lab, Los Alamos, NM, 1994

A. Le Bail, H. Duroy and J.L. Fourquet, *Mat. res. Bull.* 447, 23 (1988)

J. D. Gale, *J. Chem. Soc., Faraday Trans.*, 629, 93 (1997)

J. D. Gale, *J. Phys. Chem B*, 5423, 102 (1998)

L. N. Kantorovich, *Phys. Rev. B* 3520, 51 (1995)

L. N. Kantorovich, *Phys. Rev. B* 3535, 51 (1995)

D. J. Lacks, G. C. Rutledge, *J. Chem. Phys.*, 9961, 101, 1994

J. D. Lee, J. L. Pentecost, *J. Am. Ceram. Soc.*, 183, 59(1976)

P. Lightfoot, D. A. Woodcock, M. J. Maple, L. A. Villaesusa and P. A. Wright, *J. Mater. Chem..*, 212, 11 (2001)

J. R. Mackert, S. W. Twiggs, A. L. Williams, *J. of Dent. Res.*, 1590, 79(2000)

T.A. Mary, J.S.O. Evans, A. W. Sleight and T. Vogt, *Science*, 272, 90 (1996)

R. Mittal and S. L. Chaplot, *Phys. Rev. B* 60 (1999)

R. Mittal, S. L. Chaplot, *Solid State Communications* 319, 115 (2000)

G. D. Price, S. C. Parker and M Leslie, *Mineral. Mag.*, 157, 51 (1987)

A. K. Pryde, K. D. Hammonds, M. T. Dove, V. Heine, J. D. Gale, M. C. Warren, *J. Phys.: Condens. Matter.* 10973, 8 (1996)

A. P. Ramirez, G. R. Kowach, *Phys. Rev. Lett.* 4903, 80 (1998)

T. R. Ravindran, A. K. Aroura, T. A. Mary, *Phys. Rev. Letters*, 17, 84 (2000)

H. M. Rieveld, *Acta Crystallogr.*, 151, 22 (1967)

K. Röttger, A. Endriss, J. Ihringer, S. Doyle, and W.F. Khuss, *Acta Crystallogra.* Sect B 50, 644 (1994)

H. Schneider, O. W. Floerke, A. Majdic, Proc. Br. Ceram. Soc., 267, 28 (1979)

G. Shirane and S. Hoshina, *J. Phys. Soc. Jpn.* 6, 265 (1951)

D. Taylor, *Mineral. Mag.*, 761, 36(1968)

D Taylor, C. M. B. Henderson, *Amer. Mineral*, 1476, 53(1968)

D. Taylor, C. M. B. Henderson, *Mineral. Mag.*, 708, 52(1988)

M. B. Taylor, G. D. Barrera, N. L. Allan, T. H. K.. Barron, *Phys. Rev. B* 14380, 56 (1997)

P. Tschaufeser and S. C. Parker, *J. Phys. Chem.*. 10609, 99 (1995)

K. Voores and J. Donohue, *Acta Cryst.*, 25, 8 (1955)

G. K. White, *Contemp. Phys.* 34, 193 (1993)

D. A. Woodcock, P. Lightfoot, L. A. Villaescusa, M. Diaz-Cabanas, M. A. Camblor, D. Engberg. *J. Mater. Chem.*, 349, 9 (1999)